JOURNAL OF COMPUTATIONAL PHYSICS 121, 213–237 (1995)

Semi-Implicit Extension of a Godunov-Type Scheme Based on Low Mach Number Asymptotics I: One-Dimensional Flow

R. KLEIN

Institut für Technische Mechanik, RWTH, Templergraben 64, 52056 Aachen, Germany

Received December 20, 1993; revised March 6, 1995

A single time scale, multiple space scale asymptotic analysis provides detailed insight into the low Mach number limit behavior of solutions of the compressible Euler equations. We use the asymptotics as a guideline for developing a low Mach number extension of an explicit higher order shock-capturing scheme. This semi-implicit scheme involves multiple pressure variables, large scale differencing and averaging procedures that are discretized versions of standard operations in multiple scales asymptotic analysis. Advection and acoustic wave propagation are discretized explicitly and upwind and only one scalar elliptic equation is to be solved implicitly at each time step. This equation is a pressure correction equation for incompressible flows when the Mach number is *zero*. In the low Mach number limit, the time step is restricted by a Courant number based essentially on the maximum flow velocity. For moderate and large Mach numbers the scheme reduces to the underlying explicit higher order shock capturing algorithm.

1. INTRODUCTION

One major motivation of this work derives from a range of interesting applications in combustion science. A typical example is the deflagration-to-detonation transition, where low speed combustion dominates the initial stages, while foreign-induced or self-induced flame acceleration eventually drives the flow into the fully compressible regime (see, e.g., [1] and the references therein). A direct numerical simulation scheme for these processes should efficiently and accurately deal with both the low and high Mach number flow regime.

A considerable number of publications have been devoted to developing a computational method for low Mach number flows [2–10]. All of these methods are designed to avoid the Courant–Friedrich–Levy time step restriction for explicit schemes, which becomes extremely stringent for small Mach numbers due to the large discrepancy between the sound speed and a characteristic flow velocity. In the original governing equations one tries to separate terms that are associated with convection from others that become singular as the Mach number M vanishes and which, in the limit, induce the well-known change of type of the governing equations from hyperbolic to hyperbolic/elliptic. Such a decomposition is by no means unique and several quite different approaches have been adopted with varying success. One reason for the present work is that each of the schemes in the references cited fails to comply with at least one item from the following list of desirable features for applications in low Mach number combustion:

— The scheme should allow for large amplitude density variations as $M \to 0$.

— The split step containing the "stiff" terms, which is discretized implicitly, should be hyperbolic with a signal speed equal to the local speed of sound as $M \to 0$.

— Appropriate pressure variables should be defined that independently represent the global thermodynamic pressure and the pressure fluctuations induced by inertial forces and the divergence constraint in incompressible flows.

— The scheme should accurately describe long wave acoustics associated with pressure amplitudes $\delta p/p_\infty = O(M)$.

Ideally, the scheme would successfully simulate zero Mach number variable density flows, weakly nonlinear acoustic wave propagation at small but finite Mach numbers, and it should automatically turn into an explicit high resolution shock capturing scheme at high Mach numbers $M = O(1)$.

In this paper we consider the low Mach number asymptotic limit of the Euler equations and use the resulting insight as a guideline for designing a semi-implicit low Mach number extension of a Godunov-type MUSCL scheme for compressible flows [11, 12]. Since we develop a numerical scheme in conservation form, we use the *conservative formulation* of the Euler equations throughout the analysis.

A wide range of particular distinguished limits for wave amplitudes and wave lengths, as well as length and time scales, can be relevant in the zero Mach number limit process, depending on the specific initial and boundary data (see Refs. [13–19], which we contrast with the present results in Section 5). Here we consider a regime that is a relevant for the above-mentioned combustion applications with crucial acoustic wave effects: In a combustion device where a low-speed (turbulent) flame is the dominant driving force for the flow field, including entropy, vorticity, and acoustic fluctuations, the time scales of all the flow phenomena are dominated by the unsteady evolution of the flame front. A *single time scale/multiple space scale*

0021-9991/95 $12.00

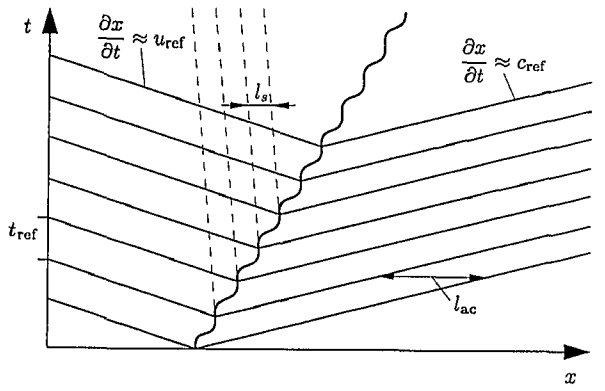

FIG. 1.1. Space–time diagram for the wave generation by an unsteady premixed flame.

asymptotic analysis of the low Mach number limit is appropriate in this case. The situation is sketched in the space–time diagram of Fig. 1.1. Let t_{ref} be a characteristic time scale for fluctuations of the flame speed and let l_s and l_{ac} denote the characteristic length scales of entropy perturbations and acoustic waves generated by the flame, respectively. These length scales may be estimated as $l_s \sim u_{ref} t_{ref}$, $l_{ac} \sim c_{ref} t_{ref}$, where u_{ref} is a characteristic flow velocity, comparable to the flame burning speed, and c_{ref} is a reference speed of sound. Obviously, $l_s \sim M l_{ac}$, with

$$M \sim \frac{u_{ref}}{c_{ref}} \ll 1. \tag{1.1}$$

This type of flow can be analyzed by a single time, two space scale asymptotic analysis involving a reference time scale t_{ref} and length scales l_{ac} and $l_{ref} := l_s$.

1.1. *Summary of the Asymptotic Analysis*

The analysis reveals several key features of the low Mach number limit process. First, it exhibits three physically distinct roles of "the" pressure as

(i) a thermodynamic variable,

(ii) an acoustic wave amplitude, and

(iii) the balancing agent for intertial forces in small scale flow structures guaranteeing compliance with a local divergence constraint.

These "roles" of the pressure have been discussed in earlier work [20, 13, 14], yet the present analysis is distinguished by the fact that all of the effects described above influence the velocity field at *leading* order and on a common time scale. In the present asymptotics, role (i) is played by the leading order pressure $p^{(0)}$, role (ii) by the first-order pressure $p^{(1)}$, and role (iii) by the second-order pressure $p^{(2)}$. For zero Mach number and for a fixed size of the flow domain, only $p^{(2)}$ retains spatial variation and it becomes "the pressure" of the incompressible flow equations satisfying the well-known Poisson equation (see [20, 14, 18] for formulations, including the influence of exothermic chemical reactions). We claim that a numerical scheme that is supposed to survive the passage to the limit $M = 0$ must allow for at least two independent pressure variables, namely the total pressure p and a field corresponding to $p^{(2)}$, if the physical effects outlined above are to be represented appropriately. When acoustic waves with order $O(M)$ pressure variation are important, as in the present work, a suitable approximation of the first-order pressure $p^{(1)}$ needs to be introduced in addition. (Currently we extract this from p through certain summation procedures, but other alternatives involving an independent array in the numerical scheme can be thought of as well.)

In the asymptotic analysis we use the conservative formulation of the governing equations whenever possible. An interesting aspect of this "asymptotics in conservation form" is the fact that the divergence constraint for the incompressible velocity field, $\nabla \cdot v = 0$, derives from the *energy equation*, but *not* from the continuity equation. In fact, the continuity equation becomes an advection equation for density fluctuations as $M \to 0$. By incorporating this knowledge in the numerical scheme we obtain a method for low speed flows with large amplitude density variations, which is conceptually very close to Chorin's [21] projection method (see [22, 30] and Section 3 below). We emphasize that the projection step corresponds, in this context, to guaranteeing an *energy* balance, instead of mass conservation, while solving the continuity equation allows one to introduce variable densities/entropies in a very natural way.

Note that variable density capabilities are a necessary feature of a scheme for combustion simulations, since thermal expansions in a flame considerably change the density. Another important aspect is that the leading order pressure becomes spatially homogeneous in the limit but may still change in time. In that case, global $O(1)$ pressure changes induce a nonzero flow divergence even as $M \to 0$. This feature is important for combustion in a closed vessel where global pressure changes are induced by the thermal expansion of the reacting gases [14, 18].

Besides multiple pressure variables and a density (and momentum) advection mechanism, the scheme incorporates discrete versions of two important operations of multiple scales asymptotics. These are averages over small scale fluctuations and large scale differentiation. The former is needed, e.g., when the first-order long wave acoustic pressure $p^{(1)}$ is to be extracted at each time step from the full pressure, $p = p^{(0)} + Mp^{(1)} + M^2 p^{(2)}$. We derive a summation formula that allows us to obtain $p^{(1)}$ from the discrete values of p *without* ever dividing by the Mach number. (Large scale differencing is the translation into a numerical discretization of the derivative with respect to a large scale variable in multiple scales asymptotics.) Let x denote the space variable resolving the small scale entropy (and vortical flow) structures and let $\xi = Mx$ be the acoustic scale variable. Then, in a two-scale asymptotic analysis, any dependent variable, $f(x, t; M)$, is expanded as

$$f(x, t; M) = f^{(0)}(x, \xi, t) + Mf^{(1)}(x, \xi, t) + M^2 f^{(2)}(x, \xi, t) + \cdots \quad (\xi = Mx). \tag{1.2}$$

A large scale derivative operator $(\partial_\xi)_{x,t}$ naturally appears in the asymptotic expansion of the governing equations, since

$$\left.\frac{\partial f}{\partial x}\right|_{t;M} = (\partial_x + M\partial_\xi)[f^{(0)} + Mf^{(1)} + M^2 f^{(2)} + \cdots]. \tag{1.3}$$

Our scheme includes a discrete version of this operator.

1.2. *Description of the Numerical Scheme*

The proposed numerical scheme is a Strang-type operator splitting technique applied to the following decomposition of the (nondimensionalized) Euler equations:

System I.

$$\begin{aligned} \rho_t + (u\rho)_x &= 0, \\ m_t + (um)_x &= 0, \end{aligned} \tag{1.4}$$

where $m \equiv \rho u$, and

System II.

$$\begin{aligned} m_t + \frac{1}{M^2} p_x &= 0, \\ e_t + (Hm)_x &= 0, \end{aligned} \tag{1.5}$$

where

$$p = (\gamma - 1)\left(e - M^2 \frac{m^2}{2\rho}\right), \quad H = \frac{e + p}{\rho}. \tag{1.6}$$

In (1.4)–(1.6) the quantities ρ, u, e, p, and H are the density, flow velocity, total energy per unit volume, pressure, and the total enthalpy per unit mass, respectively. All these quantities are nondimensional and scaled to be $O(1)$ as $M \to 0$. The details are given in (2.1)–(2.3) below.

System I represents advection of density and momentum and, via terms involving u_x, includes density changes due to acoustic waves and global background compression. A formal characteristic analysis of System II shows that it is hyperbolic with signal speeds

$$\lambda_{II}^{\pm} = \pm \frac{1}{M} c + O(1), \tag{1.7}$$

where c is the nondimensional speed of sound (with $c = O(1)$ as $M \to 0$). Thus, System II is responsible for the representation of fast acoustic wave propagation and it has the correct signal speeds to leading order in the Mach number.

Beyond this quite formal characteristic argument, the asymptotic analysis shows that System II describes, in fact, *three* physically quite distinct mechanisms, each of which deserves special attention in the numerical discretization: Mechanism number one involves global compression. Systems with characteristic dimensions comparable to l_{ref} are too small to accommodate long wave acoustics. When a change of the system volume is imposed in that case, the rapid pressure equilibration leads to a quasi-homogeneous global pressure rise (see [23, 14, 16]). Unless high frequency solution components with time scales $O(l_{ref}/c_{ref})$ are admitted, the pressure expansion is then missing an $O(M)$ contribution, i.e., $p = p^{(0)}(t) + M^2 p^{(2)}(x, t)$. Mechanism number two is the propagation of long wave acoustics. When the system dimensions are $O(l_{ref}/M)$, there is no global pressure change on the time scale l_{ref}/u_{ref}, but long wave acoustics involving $O(M)$ pressure perturbations are supported. In that case, System II describes these long wave acoustics and the appropriate multiple length scale expansion scheme for the pressure reads $p = p_0 + Mp^{(1)}(Mx, t) + M^2 p^{(2)}(x, Mx, t)$. The third mechanism is related to the divergence constraint, which plays a role in both the regimes just mentioned. The second-order pressure $p^{(2)}$ in both cases describes a local balance of forces that is responsible for guaranteeing a side constraint on the divergence of the flow field. For zero Mach number when there is no global compression this constraint is $\nabla \cdot v \equiv 0$ and $p^{(2)}$ satisfies the well-known Poisson equation for "the pressure" in incompressible flows.

Guided by the asymptotics, the discretization of System II separately accounts for all these effects. The result is a scheme that combines explicit predictor steps for long wave linear acoustics or global compression with a single implicit scalar Poisson-type corrector scheme that takes care of both acoustic nonlinearities and the divergence constraint.

Currently, we employ for System I a full explicit Godunov-type MUSCL scheme for compressible flows. It operates in a modified version to describe convection at low flow speeds and we switch to the original version for moderate and large Mach numbers. This scheme can be replaced in principle by any other shock capturing strategy. For System II we use LeVeque's large time step method [24] to describe the linearized long wave acoustics and simple central differences for the implicit $O(M^2)$ pressure correction; the latter accounting for acoustic nonlinearities as well as the divergence constraint in the limit of vanishing Mach number. The order of accuracy of the scheme is $O(M\,\Delta t, M\,\Delta x, (\Delta x)^2, (\Delta t)^2)$ for small Mach numbers in the semi-implicit version and it inherits second-order accuracy in space and time from the underlying Godunov-type MUSCL scheme for moderate and large Mach numbers.

We describe in this paper a one-dimensional version of this numerical method based on asymptotic considerations. The scheme has the following characteristics:

(1) It is a semi-implicit operator splitting technique where the first step describes advection of mass and momentum and

the second step accounts for global background compression, long wave acoustic wave propagation, and the local balance of forces.

(2) It involves two independent pressure variables that correspond to the full pressure p and to the second-order term, $p^{(2)}$, in an asymptotic expansion $p = p^{(0)} + Mp^{(1)} + M^2p^{(2)}$ as $M \to 0$. The first-order pressure $p^{(1)}$ is extracted when needed from p through suitable nonsingular summation procedures.

(3) The spatial discretization includes large scale differencing and averaging procedures that resemble corresponding standard operations of multiple scales asymptotics.

(4) For small but finite Mach numbers it treats convection and linear acoustic wave effects explicitly with an upwind discretization, while the local balance of forces and weakly nonlinear acoustic effects are accounted for in an implicit step.

(5) The implicit step involves a single Poisson type equation which, at zero Mach number, reduces to the pressure equation of a projection method, [21].

(6) The scheme allows the passage to zero Mach number with a Mach number independent time step restriction.

(7) For moderate and large Mach numbers the scheme becomes a standard explicit higher order shock capturing scheme.

(8) It is second-order accurate in space and time in the explicit Godunov-type mode and accurate of order $O(M\,\Delta t, M\,\Delta x, (\Delta x)^2, (\Delta t)^2)$ in the semi-implicit version for low Mach numbers.

The organization of this paper is as follows:

In Section 2 we discuss the single time/multiple space scale low Mach number asymptotics for the Euler equations in conservation form and in multidimensions. In Section 3 we specialize to a single space dimension and extract the specific subsets of equations that represent advection, acoustics, and the local divergence constraint. We interpret the results as a nonlocal decomposition of the Euler equations in the sense of the standard operator splitting technique. For each subset of equations we introduce a specific discretization that accounts for its mathematical character. In this fashion, we obtain a numerical method for the *full* Euler equations—*not* one for a set of simplified limit equations. The role of the asymptotic analysis in this development is to help in designing a discretization that survives the passage to zero Mach number (rather than to provide a simplified equation set). In Section 4 we present results for several test problems that document the performance of the scheme in different Mach number regimes. The examples considered include weakly nonlinear acoustic effects and pressure wave interactions at $M \approx 0.1$, the passage of a long wave acoustic pulse over a short wave, large amplitude density layering at $M \approx 0.02$ and the flow in an open tube with imposed large amplitude global compression and large spatial density variations at $M \approx 10^{-4}$. In Section 5 we provide a brief report on existing literature in the field and contrast it with the present work. Section 5.1 reviews the low Mach number asymptotics, while Section 5.2 compares various numerical techniques for low Mach number flows with our new approach.

2. LOW MACH NUMBER ASYMPTOTICS FOR THE EULER EQUATIONS IN CONSERVATION FORM

2.1. *Summary*

Here we analyze the compressible Euler equations, which in nondimensional form and for one, two, or three dimensions read

$$\begin{aligned} \rho_t + \nabla \cdot \mathbf{m} &= 0 \\ \mathbf{m}_t + \nabla \cdot \left(\mathbf{m} \circ \mathbf{v} + \frac{1}{M^2} p\, \mathbf{I} \right) &= 0 \\ e_t + \nabla \cdot (\mathbf{v}[e + p]) &= 0, \end{aligned} \tag{2.1}$$

where ρ, $\mathbf{m}$, and e, are the conserved quantities, namely mass, momentum, and total energy per unit volume, $\mathbf{v} \equiv \mathbf{m}/\rho$ is the flow velocity, p the pressure, $\mathbf{I}$ denotes the unit tensor and the $\circ$ symbol indicates the tensorial product. The pressure is related to the conserved variables through the equation of state of a perfect gas,

$$p = (\gamma - 1)\left[e - M^2 \frac{1}{2} \frac{\mathbf{m}^2}{\rho} \right] \quad \text{with} \quad \gamma = \text{const.} \tag{2.2}$$

To obtain (2.1), (2.2) we have used a nondimensional notation by defining

$$\begin{aligned} \rho &= \rho' / \rho'_{\text{ref}} \\ v &= v' / u'_{\text{ref}} \\ p &= p' / p'_{\text{ref}} \\ x &= x' / l'_{\text{ref}} \\ t &= t' u'_{\text{ref}} / l'_{\text{ref}}, \end{aligned} \tag{2.3}$$

where primes denote dimensional quantities. Note that we use a reference velocity, u'_{ref} independent of $(p'_{\text{ref}}/\rho'_{\text{ref}})^{1/2}$. This choice guarantees that the nondimensional velocity, v, remains well defined and of order $O(1)$ in the limit of a vanishing Mach number

$$M = \frac{u'_{\text{ref}}}{(p'_{\text{ref}}/\rho'_{\text{ref}})^{1/2}} \to 0. \tag{2.4}$$

We emphasize that M is a global parameter characterizing the nondimensionalization but *not* the local flow Mach number.

Also time is nondimensionalized by a characteristic flow time scale—not by a characteristic time for sound wave propagation.

We analyze the behavior of specific solutions of (2.1) which, for small Mach numbers $M \ll 1$, have an expansion

$$\mathbf{U}(x, t; M) = \mathbf{U}^{(0)} + M\mathbf{U}^{(1)} + M^2\mathbf{U}^{(2)} + o(M^2), \quad (2.5)$$

where $\mathbf{U}$ denotes the vector of the unknowns. Note that particularly the pressure has a nonzero first-order contribution, $Mp^{(1)}$. By including $O(M)$ pressure perturbations, we allow acoustic waves to affect the velocity field at the leading order. To our knowledge this regime has not before been analyzed in more than one space dimension and in the context of the zero Mach number, (quasi-)incompressible limit.

Each of the expansion functions in (2.5) depends on two space variables, i.e.,

$$\mathbf{U}^{(j)} = \mathbf{U}^{(j)}(\mathbf{x}, \boldsymbol{\xi}, t), \quad \text{where} \quad \boldsymbol{\xi} = M\mathbf{x}. \quad (2.6)$$

Here $\mathbf{x}$ resolves small scale entropy fluctuations and vortical structures, while $\boldsymbol{\xi}$ is an acoustic scale variable. We do not carry out a multiple time scale analysis involving time variables t and $\tau = Mt$, since we are interested only in translating the asymptotic behavior on the shortest time scale into a numerical scheme. The scheme will then resolve this short time scale and the numerical solution should automatically accumulate long time effects.

In this section we explore the consequences of the ansatz in (2.5). We use no more and no less than identification of terms multiplied by the same powers of the Mach number and averages over the smallest scales in order to extract important insight into the behavior of solutions upon passage to the limit $M \to 0$. Throughout the analysis we *assume* that these averages exist when needed. We are aware that this is a highly nontrivial assumption, but the idea is to use the insight obtained from this analysis to design a new conservative discretization of the *full* governing equations. Thus, we do not rely on a numerical solution of the asymptotic limit equations and we may hope that the resulting algorithm will be able to also handle more general situations, where these averages do not necessarily exist in an asymptotic sense. Their discrete analogues certainly exist in any case, since they merely involve certain summation procedures over finite subsets of the domain of integration.

Here we summarize the principal results of the asymptotics before we go into details in Section 2.2. First we will identify those two expressions in the governing equations that are responsible for the degeneration from a hyperbolic to an elliptic/hyperbolic system as the Mach number vanishes. The first term is the pressure gradient, $(1/M^2)\,\nabla p$, in the momentum equation, which induces $\nabla_{\mathbf{x}} p^{(0)} = \nabla_{\boldsymbol{\xi}} p^{(0)} = \nabla_{\mathbf{x}} p^{(1)} = 0$, so that

$$p^{(0)} \equiv P_0(t), \quad p^{(1)} \equiv P^{(1)}(\boldsymbol{\xi}, t). \quad (2.7)$$

The second singular term is the enthalpy flux divergence $\nabla \cdot (\mathbf{v}[e + p])$ in the *energy equation*. Together with the above constraints on the pressure gradient, this term introduces the global divergence condition

$$\nabla_{\mathbf{x}} \cdot \mathbf{v}^{(0)} = -\frac{1}{\gamma P_0}\frac{dP_0}{dt}. \quad (2.8)$$

(Note that the right-hand side depends on time only!) For incompressible flows, when there is no global compression, one has $\nabla_{\mathbf{x}} \cdot \mathbf{v}^{(0)} = 0$. These two terms have been identified before in a characteristic analysis by Casulli and Greenspan [3].

We will then discuss the principal role of the continuity equation. One finds

$$\rho_t^{(0)} + \mathbf{v}^{(0)} \cdot \nabla_{\mathbf{x}} \rho^{(0)} = \frac{1}{\gamma P_0}\frac{dP_0}{dt}. \quad (2.9)$$

This equation describes how each mass element is advected along its particle path while being isentropically compressed or expanded when there is a global leading over pressure variation. In particular, each mass element may have an individual initial density corresponding to a nontrivial initial entropy distribution. Thus, the asymptotics includes variable density flows in a natural way. Incidentally, the continuity equation does *not* yield the divergence-free condition in the present conservative formulation.

Finally, the asymptotic analysis of the second-order momentum and first-order energy equations shows that

(1) the *second-order* pressure $p^{(2)}$ reduces to the standard pressure variable for incompressible flows that satisfies the well-known Poisson equation as $M \to 0$ and that

(2) the first-order pressure $P^{(1)}$ appears as an acoustic wave amplitude, which under certain restrictions satisfies the linearized, nonconstant coefficient wave equation

$$P_{tt}^{(1)} - \nabla_{\boldsymbol{\xi}} \cdot (\bar{c}_0^2(\boldsymbol{\xi})\, \nabla_{\boldsymbol{\xi}} P^{(1)}) = 0, \quad (2.10)$$

where the signal velocity $\bar{c}_0 = (\gamma P_0/\bar{\rho}^{(0)}(\boldsymbol{\xi}))$ is slowly varying on the time scale considered, with P_0 from (2.7) and $\bar{\rho}^{(0)}$ the small-scale average of the leading order density distribution.

2.2. *Asymptotic Expansions, Averaging Procedures, and Interpretations*

Here we describe the hierarchy of perturbation equations that follows from the asymptotic expansion in (2.5). We selectively present only those equations that will be relevant in the further procedure of designing a numerical scheme. We do not attempt in this paper to systematically solve the asymptotic system.

The leading order continuity equation reads

$$\rho_t^{(0)} + \nabla_{\mathbf{x}} \cdot (\mathbf{v}^{(0)} \rho^{(0)}) = 0. \quad (2.11)$$

The leading, first- and second-order momentum equations are

$$\begin{aligned} \nabla_x p^{(0)} &= 0, \\ \nabla_x p^{(1)} + \nabla_\xi p^{(0)} &= 0, \\ \mathbf{m}_t^{(0)} + \nabla_x \cdot (\mathbf{m}^{(0)} \circ \mathbf{v}^{(0)}) + \nabla_x p^{(2)} &= -\nabla_\xi p^{(1)}, \end{aligned} \tag{2.12}$$

and the set of energy equations is

$$\begin{aligned} e_t^{(0)} + \nabla_x \cdot (\mathbf{v}h)^{(0)} &= 0, \\ e_t^{(1)} + \nabla_x \cdot (\mathbf{v}h)^{(1)} &= -\nabla_\xi \cdot (\mathbf{v}h)^{(0)}, \\ e_t^{(2)} + \nabla_x \cdot (\mathbf{v}h)^{(2)} &= -\nabla_\xi \cdot (\mathbf{v}h)^{(1)}, \end{aligned} \tag{2.13}$$

where $h = e + p = \rho H$ is the total enthalpy per unit volume.

The first two equations in (2.12) are the first to indicate the change of type of the governing equations upon transition from the compressible to the incompressible regime. These equations do not involve a time derivative, so that they are of elliptic type. In an asymptotic approach, one first concludes from $(2.12)_1$ that $p^{(0)} = P^{(0)}(\xi, t)$. Then the $\mathbf{x}$-average of $(2.12)_2$, with the requirement of sublinear growth of $p^{(1)}$ as $|\mathbf{x}|$ becomes large, yields

$$\begin{aligned} p^{(0)} &= P_0(t), \\ p^{(1)} &= P^{(1)}(\xi, t). \end{aligned} \tag{2.14}$$

Considering next the leading order energy equation $(2.13)_1$, thereby taking into account $(2.14)_1$ and the equation of state (2.2), one finds that

$$\nabla_x \cdot \mathbf{v}^{(0)} = -\frac{1}{\gamma P_0} \frac{dP_0}{dt}. \tag{2.15}$$

We discuss two very different, yet equally important regimes and draw conclusions from (2.15). In the first regime, we assume that the overall system dimensions are comparable to the reference length l'_{ref} from (2.3). Then we have a single-length scale solution and the large scale variable ξ becomes void. Detailed analyses of this regime including also the influence of exothermic chemical reactions are given in [14, 18]. Equation (2.15) may then be integrated with respect to $\mathbf{x}$ to yield

$$\frac{d \ln P_0^{1/\gamma}}{dt} = -\frac{1}{V} \int_{\partial V} \mathbf{v}^{(0)} \cdot \mathbf{n} \, d\sigma, \tag{2.16}$$

where V denotes the volume, ∂V is the boundary of the physical domain considered, and $\mathbf{n}$ is the outer unit normal on ∂V. If the normal velocity $\mathbf{v}^{(0)} \cdot \mathbf{n}$ is known from boundary conditions all along ∂V, then this equation yields the overall pressure rise due to compression from the boundaries. A typical example for this kind of situation is a closed piston–cylinder system, where the piston motion determines the global pressure rise. If, on the other hand, the pressure is imposed at least on part of the boundary, then, due to spatial homogeneity of P_0, Eq. (2.16) yields an integral constraint on the normal velocities along ∂V. In both cases (2.15), together with (2.16) represents a second equation that exhibits a nontrivial change of type of the governing equations: The flow divergence $\nabla_x \cdot \mathbf{v}^{(0)}$ is either determined by the volume flux across the boundary at any time, i.e.,

$$\nabla_x \cdot \mathbf{v}^{(0)} = \frac{1}{V} \int_{\partial V} \mathbf{v}^{(0)} \cdot \mathbf{n} \, d\sigma, \tag{2.17}$$

or it is imposed from the outside by $O(1)$ pressure changes on the boundary. In that case the right-hand side of (2.15) is explicitly prescribed.

In the second regime for characteristic system dimensions the system is large compared to l'_{ref} and the acoustic scale variable ξ carries nontrivial information. Then the volume average with respect to $\mathbf{x}$ of (2.15) yields

$$0 = -\frac{1}{\gamma P_0} \frac{dP_0}{dt}, \tag{2.18}$$

and P_0 is invariant on the time scale considered. On the other hand, inserting (2.18) back into (2.15) one finds the small-scale divergence constraint

$$\nabla_x \cdot \mathbf{v}^{(0)} = 0. \tag{2.19}$$

It seems remarkable that in the present formulation of the asymptotics *in conservation form,* the divergence condition for incompressible flows follows from the *energy equation* but not from the continuity of mass. In fact, the continuity equation (2.11) plays a quite different role. It may be rewritten as

$$\rho_t^{(0)} + \mathbf{v}^{(0)} \cdot \nabla_x \rho^{(0)} = -\rho^{(0)} \nabla_x \cdot \mathbf{v}^{(0)}. \tag{2.20}$$

In the first scenario this equation yields

$$\frac{D \ln \rho^{(0)}}{Dt} = \frac{1}{\gamma} \frac{d \ln P_0}{dt}, \quad \text{where} \quad \frac{D}{Dt} = \partial_t + \mathbf{v}^{(0)} \cdot \nabla_x, \tag{2.21}$$

which is the equation for quasi-static adiabatic compression of mass elements along particle paths. This result indicates that $P_0(t)$ operates as a thermodynamic pressure variable as announced in the Introduction. In the second scenario with multiple length scales, where $\nabla_x \cdot \mathbf{v}^{(0)} \equiv 0$, Eq. (2.21) simply describes the advection of the leading order density distribution.

Consider next the second-order momentum equation, $(2.12)_3$. Again we distinguish the two scenarios mentioned above. For the single length scale case the right-hand side vanishes identically and one obtains the standard momentum equation for zero Mach number flows [20, 14],

$$\mathbf{m}_t^{(0)} + \nabla_x \cdot ((\mathbf{m} \circ \mathbf{v})^{(0)} + p^{(2)} \mathbf{I}) = 0. \tag{2.22}$$

The second-order pressure $p^{(2)}$ then must be the balance-of-forces agent that ensures compliance with the divergence constraint (2.15).

The situation becomes more involved in the multiple length scale regime. Then the term $\nabla_\xi P^{(1)}$ is present in the momentum balance and its effect needs to be studied. We separate the small-sale and acoustic scale balance of forces by volume averaging $(2.12)_3$ over $\mathbf{x}$. This yields

$$\overline{(\rho \mathbf{v})_t^{(0)}} + \nabla_\xi P^{(1)} = 0, \tag{2.23}$$

where the overbar denotes the small-scale average. To see the physics of this equation we combine (2.23) with the small-scale average of the first-order energy equation $(2.13)_2$. Taking into account that

$$e^{(0)} = \frac{1}{\gamma - 1} P_0, \tag{2.24}$$

we find that

$$P_t^{(1)} + \gamma P_0 \nabla_\xi \cdot \overline{\mathbf{v}_0} = 0, \quad \text{where} \quad \overline{\mathbf{v}_0} = \overline{\mathbf{v}^{(0)}}. \tag{2.25}$$

Consider now a flow that has $O(1)$ density variation only on the acoustic scale, so that

$$\rho^{(0)} \equiv \overline{\rho}_0(\boldsymbol{\xi}, t). \tag{2.26}$$

Then the small scale average of equation (2.20) yields

$$\overline{\rho}_{0,t} \equiv 0, \tag{2.27}$$

saying that $\overline{\rho}_0$ can vary only on time scales much longer than the reference time $t'_{\text{ref}} = l'_{\text{ref}}/u'_{\text{ref}}$. Indeed, since the density distribution is mainly advected by the flow, nontrivial changes of $\overline{\rho}_0$ can occur only when mass elements have passed $O(l'_{\text{ref}}/M)$ distances, i.e., over times of order t'_{ref}/M. Using (2.26), (2.27), one obtains

$$\overline{(\rho \mathbf{v})_t^{(0)}} = \overline{\rho}_0(\boldsymbol{\xi}) \overline{\mathbf{v}_{0,t}} \tag{2.28}$$

for the time-dependence term in (2.23). Equations (2.25)–(2.28) yield the system of nonconstant coefficient linearized acoustics,

$$\overline{\mathbf{v}_{0,t}} + (1/\overline{\rho}_0(\boldsymbol{\xi}))\, \nabla_\xi P^{(1)} = 0,$$
$$P_t^{(1)} + \gamma P_0 \nabla_\xi \cdot \overline{\mathbf{v}_0} = 0.$$

This system yields the wave equation for $P^{(1)}$,

$$P_{1,tt} - \nabla_\xi \cdot (c_0^2(\boldsymbol{\xi})\, \nabla_\xi P^{(1)}) = 0, \tag{2.30}$$

where

$$c_0^2(\boldsymbol{\xi}) = \frac{\gamma P_0}{\overline{\rho}_0(\boldsymbol{\xi})} \tag{2.31}$$

is the relevant average speed of sound. If one allows for $O(1)$ variations of the leading order density on the small reference length scale, the interesting result is that the system of linearized acoustics is not retrieved automatically. With the separation of $\rho^{(0)}$, $\mathbf{v}^{(0)}$ into $\mathbf{x}$-scale fluctuations and $\boldsymbol{\xi}$-scale averages according to

$$\rho^{(0)} = \tilde{\rho}^{(0)}(\mathbf{x}, \boldsymbol{\xi}, t) + \overline{\rho}^{(0)}(\boldsymbol{\xi})$$
$$\mathbf{v}^{(0)} = \tilde{\mathbf{v}}^{(0)}(\mathbf{x}, \boldsymbol{\xi}, t) + \overline{\mathbf{v}}^{(0)}(\boldsymbol{\xi}, t), \tag{2.32}$$

one has

$$\overline{\rho^{(0)} \mathbf{v}_t^{(0)}} = \overline{\rho}^{(0)} \overline{\mathbf{v}}_t^{(0)} + \overline{(\tilde{\rho} \tilde{\mathbf{v}})_t^{(0)}}, \tag{2.33}$$

and the second term yields a nontrivial contribution. A numerical scheme that is supposed to handle this kind of situation must carefully account for this additional term. However, in this paper we will only outline the design of a numerical method for a single space dimension, in which case $\tilde{\mathbf{v}}^{(0)} \equiv 0$. This result will be discussed in more detail in the next section.

This finishes the analysis of Eqs. (2.11) through (2.13), except for a discussion of the second-order energy equation $(2.13)_3$. We observe that this equation accounts for weakly nonlinear effects through the asymptotic representation of the enthalpy flux contributions $(\mathbf{v}h)^{(1)}$, $(\mathbf{v}h)^{(2)}$ and due to the fact that $e^{(2)}$ includes the quadratically nonlinear kinetic energy term according to (2.2). We use this aspect in the numerical scheme in that we approximate the long wave acoustics by a *linear* explicit large time step predictor and capture weakly nonlinear effects successfully by a careful formulation of the implicit pressure correction equation that yields the numerical second-order pressure. We demonstrate the performance of the scheme on problems of weakly nonlinear acoustics in Section 4.

Even though it is quite tempting we resist at this point the challenge to go one step further in the multiple-scales asymptotics and derive evolution equations for all variables on the larger $\tau = Mt$ time scale. This analysis would definitely be of interest in itself, but it would dilute our main argument. As stated in the introduction to this section we intend to use the single-time scale, multiple space scale equations of this section in order to derive a new numerical scheme that in detail resolves the t'_{ref}-time scale. By incorporating a discretization of the *full equations*—not the asymptotic limit equations—we hope to obtain a scheme that automatically generates the long time accumulation effects that in an asymptotic analysis would be described by the τ-scale equations.

3. OPERATOR SPLITTING AND DISCRETIZATION IN ONE SPACE DIMENSION

Based on the asymptotic analysis of the last section we can now motivate the operator splitting into a convection system for mass and momentum:

System I.

$$\begin{aligned} \rho_t + (u\rho)_x &= 0, \\ m_t + (um)_x &= 0, \end{aligned} \tag{3.1}$$

where $u = m/\rho$, and a combined momentum/energy balance that simultaneously describes (i) the local balance of forces that ensures compliance with the divergence constraint in the zero Mach number limit and (ii) either long wave acoustics with the correct signal speeds $\pm c/M$ as $M \to 0$ or a global compression in systems that are too small to accommodate long wave acoustic pulses.

System II.

$$\begin{aligned} m_t + \frac{1}{M^2} p_x &= 0, \\ e_t + (Hm)_x &= 0. \end{aligned} \tag{3.2}$$

System I should be discretized explicitly and in an upwind fashion. System II should be discretized by a semi-implicit scheme in order to account for its mixed hyperbolic/elliptic character which results from the two submechanisms mentioned above. To allow the passage to zero Mach number we have to introduce separate pressure variables according to the asymptotic expansion $p = p^{(0)} + Mp^{(1)} + M^2 p^{(2)}$ as discussed in the previous section. Two additional requirements are imposed. First, the discretization of System I should be a suitable modified version of an explicit compressible flow solver to which the whole scheme reduces for sufficiently large Mach numbers. Second, the semi-implicit discretization of System II should minimize the damping of long wave acoustics while still allowing large time steps with Courant numbers CFL $= O(1/M)$ as $M \to 0$.

3.1. *Averaging Procedures and Multiple Pressure Variables*

Here we discuss the discrete large scale averaging procedures that we use to extract the long wave acoustic components of the solution at every time step and that define the formal pressure decomposition in terms of powers of the Mach number.

First we introduce the spatial averaging operator

$$\langle f \rangle_{\Delta,\varepsilon}(x) = \frac{\varepsilon}{2\Delta} \int_{x-\Delta/\varepsilon}^{x+\Delta/\varepsilon} f(x')\, dx', \tag{3.3}$$

which is characterized by two parameters $\Delta \ll 1$ and $\varepsilon \ll 1$. Then we define numerical acoustic and super-acoustic scale averages by

$$\begin{aligned} \bar{f}(x) &= \langle f \rangle_{\Delta x/2,M}(x), \\ \bar{\bar{f}}(x) &= \langle f \rangle_{\Delta x/2,M^2}(x). \end{aligned} \tag{3.4}$$

When the averaging domain in these expressions exceeds a given fraction of the numerical domain of integration, the localized averages are replaced by averages over all of the computational domain. This will be the case for the super-acoustic scale averages in all of the examples in Section 4.

Next we introduce three pressure variables $\bar{\bar{p}}^{(0)}, \bar{p}^{(1)}, \tilde{p}^{(2)}$, which closely correspond to the asymptotic pressure expansion functions of Section 2, by

$$\begin{aligned} \bar{\bar{p}}^{(0)} &= \bar{\bar{p}}, \\ \bar{p}^{(1)} &= \frac{1}{M}(\bar{p} - \bar{\bar{p}}), \\ \tilde{p}^{(2)} &= \frac{1}{M^2}(p - \bar{\bar{p}}^{(0)} - M\bar{p}^{(1)}). \end{aligned} \tag{3.5}$$

Obviously, we have

$$p = \bar{\bar{p}}^{(0)} + M\bar{p}^{(1)} + M^2\tilde{p}^{(2)}. \tag{3.6}$$

With this decomposition of the pressure the equation of state in (2.2), when specialized for one space dimension, becomes

$$\begin{aligned} e &= e^{(0)} + Me^{(1)} + M^2 e^{(2)} \\ &= \frac{\bar{\bar{p}}^{(0)}}{\gamma - 1} + M\frac{\bar{p}^{(1)}}{\gamma - 1} + M^2\left[\frac{\tilde{p}^{(2)}}{\gamma - 1} + \frac{\rho u^2}{2}\right]. \end{aligned} \tag{3.7}$$

Note that in computing $\bar{p}^{(1)}$ by, say, the trapezoidal rule the factors of $1/M$ from $(3.5)_2$ and $M = \varepsilon$ from the definition of the average $\langle\cdot\rangle_{M,\Delta x/2}$ cancel and we obtain the first-order pressure without ever having to divide by the Mach number. An analogous formula does not exist for $\tilde{p}^{(2)}$, so that the formula in $(3.5)_3$ cannot be used for values of M^2 comparable to machine accuracy. The quantity $M^2\tilde{p}^{(2)}$, however, *is* available and will be used in the numerical discretization.

3.2. *Convection of Mass and Momentum*

The scheme used here to discretize System I from (3.1) is admittedly not the most efficient one, but it does have the desired feature that it is equivalent to a full explicit Euler solver as the Mach number exceeds a prechosen threshold value. In case that all flows to be simulated are in the low Mach number regime a specialized more efficient method should be employed [22, 30].

We motivate the design of the scheme by a characteristic analysis of the auxiliary

System I*.

$$\begin{aligned} \rho_t + (u\rho)_x &= 0, \\ m_t + (um)_x + p_x &= 0, \\ e_t + (u[e + \bar{\bar{p}}_{\mathrm{NL}} + M^2 p])_x &= 0, \end{aligned} \tag{3.8}$$

where

$$\bar{\bar{p}}_{\mathrm{NL}} = \bar{\bar{p}} - M^2 p \tag{3.9}$$

is a nonlocal pressure contribution considered to be given and fixed in the following characteristic analysis of (3.8).

Note that the factor of $1/M^2$ multiplying the pressure gradient in the momentum equation in (2.1) is missing in the auxiliary system (3.8). Therefore (3.8) is a modification of System I in (3.1) rather than being close to the one-dimensional version of the original Euler equations from (2.1).

System I* is hyperbolic with signal speeds

$$\lambda_{\pm}^{*} = u \pm c_{*} \quad \text{with } c_{*}^2 = -\frac{E_\rho - \bar{\bar{p}}/\rho^2}{E_p}, \tag{3.10}$$

where $E(p, \rho)$ is the thermal energy per unit mass of gas defined by $E = e/\rho - M^2u^2/2$ (see also Appendix I.1). Note that both u and c_* are nondimensional and $O(1)$ as $M \to 0$. As a consequence,

$$\lambda_{\pm}^{*} = O(1) \quad \text{as} \quad M \to 0. \tag{3.11}$$

In Appendix I we present a Godunov-type discretization of System I* based on the Harten, Lax, van Leer, Einfeldt approach [25, 26]. The scheme automatically solves the original Euler equations for $M = 1$, since in that case $\bar{\bar{p}} \equiv p$ according to the definition in (3.5).

The fluxes of mass and momentum for System I* are highly accurate approximations of the fluxes for the target system I in (3.1), provided that the scaling assumptions for spatial variations of the pressure outlined in (2.5), (2.6), and (2.14) are satisfied. In that case the fluxes are accurate except for an $O(M^2)$ contribution from the pressure gradient in the momentum equation. We introduce a correction to this error in the implicit second step of the scheme.

The discretization of System I* also yields approximate enthalpy fluxes. In all of the computations presented in Section 4 we have simply neglected this information and solved the energy equation completely in the second semi-implicit step. An area of problems where the enthalpy fluxes for System I* should be used are transition problems, where the Mach number continuously increases and the solution leaves the low Mach number regime. The scheme should then smoothly transfer from the semi-implicit to the fully explicit mode, thereby shifting the task of solving the energy balance from the implicit to the explicit step. We plan to address this issue in more detail in future work.

Incidentally, System I* remains hyperbolic with signal speeds

$$\lambda_{\pm}^{*,\varepsilon} = u \pm \varepsilon(M) c_{*} \tag{3.12}$$

for any function $\varepsilon(M) = o(1)$ as $M \to 0$, if one replaces

$$p_x \quad \text{with} \quad (\varepsilon^2/M^2) p_x \tag{3.13}$$

in the momentum equation and

$$(u[e + \bar{\bar{p}}_{\mathrm{NL}} + M^2 p])_x \quad \text{with} \quad (u[e + \bar{\bar{p}}_{\mathrm{NL}}^{\varepsilon} + \varepsilon^2 p])_x \tag{3.14}$$

in the energy equation, where

$$\bar{\bar{p}}_{\mathrm{NL}}^{\varepsilon} = \bar{\bar{p}} - \varepsilon^2 p. \tag{3.15}$$

This argument may be important for a multidimensional extension of the scheme, where $\varepsilon(M) = M^{2d}$ and d is the number of space dimensions. Note that a similar argument has also been used with success in [27] to derive a semi-implicit Roe-type scheme [28] for the Euler equations.

3.3. *Explicit Predictor for Linearized Acoustics and Global Compression*

We solve System II in two steps. First we assess the effects of global compression or long wave acoustics in an explicit predictor step and then we complete the discretization by an implicit pressure correction. The key new idea as compared to standard pressure correction schemes (see, e.g., [2, 4]) is to let this *explicit* predictor provide all changes of the pressure to orders $O(\Delta t)$ and/or $O(M\,\Delta t)$, so that the implicit correction step only needs to account for higher order $O(M^2\,\Delta t)$ pressure contributions due to weak acoustic nonlinearities and the local force balance guaranteeing compliance with the divergence constraint. In this fashion we obtain a scheme that allows large time steps of order $O(1/M)$ as $M \to 0$ but nevertheless shows very low damping for long wave acoustics. We describe the explicit predictions in the present subsection and the implicit scheme for the second order pressure in the next.

To assess the influence of long wave acoustics in case that the system dimensions are of order $O(l_{\mathrm{ref}}/M)$ we compute preliminary time updates of an averaged momentum and of the first-order pressure $\bar{p}^{(1)}$ for each numerical cell by applying an explicit large time step method to the linear acoustic system

$$\left.\begin{aligned} \bar{m}_t + \bar{p}_{\xi}^{(1)} &= 0 \\ \bar{p}_t^{(1)} + (\bar{\bar{c}}^2 \bar{m})_{\xi} &= 0 \end{aligned}\right\}, \quad \text{where} \quad \xi \equiv Mx. \tag{3.16}$$

Note that this system is hyperbolic with signal speeds $\bar{\bar{c}}/M$ in the x,t-space, so that a suitable large time step discretization is needed to overcome the Courant–Friedrich–Levy condition for standard explicit schemes. To prepare for this discretization, we first generate suitable initial data $\overline{m}_j$ for the averaged momentum in each cell from the density, velocity, and pressure data at the current time level. Several possibilities for this procedure can be thought of and have been tested. The most satisfactory results have been obtained by defining

$$\overline{m}_j^n = \{\overline{u}(\bar{\bar{\rho}} + M\overline{p}^{(1)}/\bar{\bar{c}}^2)\}_j^n, \tag{3.17}$$

where $\overline{u}$, $\overline{\rho}$, and $\bar{\bar{\rho}}$ are simple acoustic and super-acoustic scale averages and

$$\bar{\bar{c}}^2 = \gamma\bar{\bar{p}}^{(0)}/\overline{\rho}. \tag{3.18}$$

The $O(M)$ contribution in the estimate of the density in (3.17) accounts for isentropic density changes due to the long wave acoustics associated with $\overline{p}^{(1)}$.

The linear acoustic predictor involves time steps of $O(\Delta t)$ for the system in (3.16) independent of the Mach number. Thus, within a time step an acoustic wave travels distances in ξ,t-space of order $\mathcal{L}^{(\xi)} = O(\bar{\bar{c}}\,\Delta t) \approx \Delta x$, which corresponds to distances in x,t-space of order $\mathcal{L}^{(x)} \approx \Delta x/M$. Thus, a wave passes about $1/M$ numerical cells of size Δx during a time step. We note that the system in (3.16) is linear, so that acoustic information may be distributed among the cells by simple superposition. LeVeque [24] proposes a large time step method for hyperbolic systems which elegantly combines conservation with a characteristic-type discretization. The key idea is to solve the local linearized Riemann problems at cell interfaces as in a standard Godunov type scheme, but to distribute the resulting jump discontinuities over the complete domain of influence of the local Riemann problem. In this way a wave generated at a cell interface may traverse several numerical grid cells in the neighborhood in one time step and the Courant–Friedrich–Levy time step restriction is avoided. A disadvantage of the method is that nonlinear wave interactions are neglected during a time step.

Here we are in the fortunate position that the system in (3.16) is in fact linear, so that the superposition principle holds exactly. Currently we use a first-order version of LeVeque's method which we describe in Appendix II. We are aware that this method does not easily transfer to more than one dimension and we are concentrating on deriving a suitable similarly simple, yet easily multi-D extendable scheme in our current work.

The results of the linear acoustic predictor are preliminary updates of energy and momentum

$$\delta e_j = M\delta e_j^{(1)} = \frac{M}{\gamma - 1}\,\delta\bar{\bar{p}}_j^{(1)}, \quad \delta\overline{m}_j. \tag{3.19a}$$

These are separately stored and then used in the implicit computation of the second-order pressure as described in the next subsection.

In (2.15)–(2.19) we discussed a single length scale regime where the characteristic lengths of acoustic waves would exceed the system dimensions considerably. An outer imposed pressure change or a global compression due to a change of volume of a closed system could, in this case, induce leading order changes of the total energy, while there would be no large scale pressure gradients contributing to the flow acceleration. In that case δe_j and $\delta\overline{m}_j$ are replaced with

$$\delta e_j = \delta e_j^{(0)} = \frac{1}{\gamma - 1}\,\delta\bar{\bar{p}}_j^{(0)}, \quad \delta\overline{m}_j \equiv 0, \tag{3.19b}$$

with $\delta\bar{\bar{p}}_j^{(0)}$ computed using (2.16) and velocity boundary data or directly the imposed boundary pressure if applicable.

3.4. *Implicit $O(M^2)$ Pressure Correction*

In this step we account for the effect on the momentum of the small scale pressure gradient $\tilde{p}_x^{(2)}$ and we obtain final $O(M^2)$ corrections for the time update of the total energy. The effects of the small scale pressure gradient on the momentum ensure compliance with a divergence constraint in the zero Mach number limit, while the $O(M^2)$ energy updates, associated with changes of $p^{(2)}$ and of the momentum, are weakly nonlinear corrections to the linear acoustic prediction discussed in the previous subsection. Formally, we solve the system

$$\begin{aligned} m_t + (p^{(2)} - p)_x &= 0, \\ M^2 e_t^{(2)} + (uh)_x &= -e_t^{\text{expl}}, \end{aligned} \tag{3.20}$$

over one time step, where an approximation to $(e_t^{\text{expl}})_j$ is known from previous calculations as $\delta e_j/\Delta t$ and $e_t^{(2)}$ includes the above-mentioned changes of the second-order pressure as well as of the kinetic energy. Note the appearance of $-p_x$ in $(3.20)_1$ which corrects the error introduced in the convection step by replacing the System I from (3.1) with the System I* from (3.8).

We will now summarize the implicit discretization of (3.20) and append important remarks and theoretical considerations at the end of this subsection. In the following the superscripts ^{0} and ^{1} denote state variables before and after application of the solution operator for System II, respectively. The *-superscript denotes the preliminary half-time updates

$$\begin{aligned} \rho_j^* &= \rho_j^0, \\ m_j^* &= m_j^0 + \tfrac{1}{2}\delta\overline{m}_j, \\ e_j^* &= e_j^0 + \tfrac{1}{2}\delta e_j \end{aligned} \tag{3.21}$$

of the conserved quantities with δe_j and $\delta\overline{m}_j$ from (3.19) and we will further use the derived quantities

$$h_j^* = e_j^* + p_j^0 + \tfrac{1}{2}(\gamma - 1)\,\delta e_j. \tag{3.22}$$

Note that the density is unaffected by System II. This justifies the notation in $(3.21)_1$ and implies that $\rho_j^1 \equiv \rho_j^0$. The conservative time update for System II now reads

$$\begin{aligned} m_j^1 - m_j^0 &= \delta\overline{m}_j - \lambda(\pi_{j+1/2}^{n+1/2} - \pi_{j-1/2}^{n-1/2}), \\ e_j^1 - e_j^0 &= \delta e_j - \lambda((m^{n+1/2}H^*)_{j+1/2} - (m^{n+1/2}H^*)_{j-1/2}), \end{aligned} \tag{3.23}$$

where $\lambda = \Delta t/\Delta x$ and

$$\begin{aligned} \pi_{j+1/2}^{n+1/2} &= \tfrac{1}{2}(p_j^{(2)} + p_{j+1}^{(2)})^1 - \tfrac{1}{2}(p_j + p_{j+1})^0, \\ H_{j+1/2}^* &= (h_j^* + h_{j+1}^*)/(\rho_j^* + \rho_{j+1}^*), \\ m_{j+1/2}^{n+1/2} &= \tfrac{1}{2}(m_j^* + m_{j+1}^*) + \delta m_{j+1/2}^{n+1/2}, \\ \delta m_{j+1/2}^{n+1/2} &= -\lambda((p_{j+1}^{(2)} - p_j^{(2)})^1 - (p_{j+1} - p_j)^0). \end{aligned} \tag{3.24}$$

Here the second-order pressure $(p_j^{(2)})^1$ from the new time level appears and before the update (3.23) can be evaluated this quantity is to be solved for. Note that the update for System II is *conservation form*, provided δe_j and $\delta\overline{m}_j$ are computed in a conservative fashion. This is the case for our code, as it uses LeVeque's [24] method.

In deriving a closed form equation for $(p_j^{(2)})^1$, we need to take into account that changes of both $p^{(2)}$ and m contribute to the energy e to order $O(M^2)$. Thus, we insert

$$e_j^1 - e_j^0 = \delta e_j + M^2\,\delta e_j^{(2)} \tag{3.25}$$

with

$$\delta e_j^{(2)} = \frac{1}{\gamma - 1}((p_j^{(2)})^1 - (p_j^{(2)})^0) + \frac{1}{2}\left(\left(\frac{m^2}{\rho}\right)^1 - \left(\frac{m^2}{\rho}\right)^0\right)_j \tag{3.26}$$

into $(3.23)_2$, thereby approximating the change of kinetic energy by

$$\delta e_{\mathrm{kin},j} \equiv \frac{1}{2}\left(\left(\frac{m^2}{\rho}\right)^1 - \left(\frac{m^2}{\rho}\right)^0\right)_j = \frac{1}{2\rho_j^0}[(m_j^0 + \delta m_j^*)^2 - (m_j^0)^2], \tag{3.27}$$

where

$$\delta m_j^* = \tfrac{1}{2}(\delta m_{j+1/2}^{n+1/2} + \delta m_{j-1/2}^{n+1/2}) + \delta\overline{m}_j \tag{3.28}$$

with $\delta m_{j+1/2}^{n+1/2}$ from $(3.24)_4$. This yields an implicit *nonlinear* equation for $(p_j^{(2)})^1$:

$$\begin{aligned} H_{j+1/2}^*(p_{j+1}^{(2)})^1 - \left(H_{j+1/2}^* + H_{j-1/2}^* + \frac{M^2}{\lambda^2(\gamma - 1)}\right)(p_j^{(2)})^1 \\ + H_{j-1/2}^*(p_{j-1}^{(2)})^1 = R_j^* + \frac{M^2}{\lambda^2}\,\delta e_{\mathrm{kin},j}. \end{aligned} \tag{3.29}$$

Here the quantity R_j^*, which collects all the explicit information, is given by

$$\begin{aligned} R_j^* &= -\frac{M^2}{\lambda^2(\gamma - 1)}(p_j^{(2)})^0 + \frac{1}{\lambda^2}\,\delta e_j \\ &\quad + \frac{1}{\lambda}((H^*\tilde{m})_{j+1/2} - (H^*\tilde{m})_{j-1/2}) \\ \tilde{m}_{j+1/2} &= \tfrac{1}{2}(m_j^* + m_{j+1}^*) + \lambda((p_{j+1} - p_j)^0). \end{aligned} \tag{3.30}$$

The (weak) nonlinearity enters through the kinetic energy term on the r.h.s. of (3.28). It is efficient to account for this term by straightforward iteration. The convergence is the faster the smaller the Mach number. The iteration (iteration counter "ν") starts with $\delta e_{\mathrm{kin},j}^{\nu=0} = 0$. The linearized equation (3.28) is solved and, given the νth iteration $(p_{j+1}^{(2)})^{1,\nu}$ for the second-order pressure, the kinetic energy term is updated using (3.27) and $(3.24)_{3,4}$ with $(p_j^{(2)})^1$ replaced with $(p_j^{(2)})^{1,\nu}$.

This concludes the presentation of our low Mach number discretization except for the following few theoretical comments and a discussion of boundary conditions. We defer the latter issue to Section 4, where we explain the boundary conditions in conjunction with the specific test problems.

We remark that:

(i) Equation (3.23) contains an adverse pressure gradient term via $(p_{j+1} - p_j)^0$. This term is introduced to correct the artificial pressure term in the advection scheme for mass and momentum in the auxiliary System I* (see $(3.8)_2$).

(ii) For zero Mach number (3.29) reads

$$\begin{aligned} \frac{(p_{j+1}^{(2)})^1 - (p_j^{(2)})^1}{\rho_{j+1}^0 + \rho_j^0} - \frac{(p_j^{(2)})^1 - (p_{j-1}^{(2)})^1}{\rho_j^0 + \rho_{j-1}^0} &= \frac{1}{\lambda}(\tilde{u}_{j+1/2} - \tilde{u}_{j-1/2}) \\ &\quad + \frac{1}{\lambda^2}\frac{1}{\gamma p}\,\delta p, \end{aligned} \tag{3.31}$$

where $\delta p \equiv (\gamma - 1)\delta e_j$ is the spatially homogeneous background pressure change and $\tilde{u}_{j+1/2} = 2\tilde{m}_{j+1/2}/(\rho_{j+1/2}^0 + \rho_j^0)$. To arrive at this equation we have used the fact that, in the limit of $M = 0$ and for fixed size of the computational domain on the convective length scale, the pressure becomes spatially homogeneous. It follows that also the enthalpies h_j^* approach $\gamma\overline{p}/(\gamma - 1)$ and hence become constant in space.

As discussed above, the replacement of System I by System

I* to describe the effects of convection will guarantee a nonsingular behavior of that part of the scheme as the Mach number is set to zero. The results in the next section indicate that the convection of density and momentum is in fact approximated with high accuracy by this method.

Equation (3.31) is the pressure equation of a projection method. The (second order) pressure $p^{(2)}$ is adjusted so as to correct any error in the flow divergence that may have been introduced during the convection step. In formulating this equation the divergence is expressed here through differences of the *cell interface velocities* $\tilde{u}_{j+1/2}$. References [22, 29] provide a more detailed analysis of the zero Mach number limit for discretizations of the compressible flow equations in the context of the present approach using low Mach number asymptotic analyses in designing the numerical scheme. The authors show that a numerical scheme that does not rely on multiple pressure variables, but only knows the thermodynamic pressure field p, *must* fail in the incompressible limit. The appropriate implicit pressure equation in that case reduces to the Laplace equation with constant boundary data, so that the unique solution is the trivial spatially homogeneous one. Consequently, such a scheme must rely on subtle differences of large numbers to describe the pressure fluctuations that in the incompressible limit guarantee the divergence condition and it is impossible to pass to the limit. (See also Section 5.2 below.)

The reader interested in particular in modern high-accuracy finite difference techniques for the numerical treatment of the zero Mach number limit equations (for reacting and nonreacting flows) should also refer to the overview and research paper by Colella [30].

4. RESULTS

In this section we demonstrate the performance of our scheme on three test problems. Each test focuses on a particular feature of solutions of the Euler equations for small Mach numbers.

In Case I we test the scheme on a problem of colliding acoustic pulses in a regime ($M \approx 0.1$), where weakly nonlinear wave deformation is important. Case II demonstrates that large amplitude, short wave length density fluctuations are properly advected with very low dissipation at $M \approx 0.02$, while at the same time a (weakly nonlinear) longwave acoustic wave train passes the density layering. Case III shows numerical results for extremely low Mach numbers ($M \approx 10^{-4}$). Again we show proper advection of a nontrivial density structure and, in addition, the influence of a large amplitude background pressure variation.

In all tests the time step is consistently limited by stability constraints for the explicit advection step as discussed in connection with (3.8)–(3.11). In dimensional notation we have

$$\frac{\Delta t'}{\Delta x'} \leq (u' + Mc')^{-1}.$$

As a consequence the effective CFL-numbers for tests I, II, III are $\mathrm{CFL_I} \simeq 5$, $\mathrm{CFL_{II}} \simeq 22$, $\mathrm{CFL_{III}} \simeq 0.5 \times 10^4$, while $\mathrm{M_I} \simeq 0.1$, $\mathrm{M_{II}} \simeq 0.02$, $\mathrm{M_{III}} \simeq 10^{-4}$. For cases I, II we test the accuracy of the scheme by comparison with numerical solutions obtained with the explicit second-order MUSCL version of the code. For case III we compare with the leading order asymptotic solution for $M \to 0$.

In all tests we consider an ideal gas with constant specific heats and an isentropic exponent $\gamma = 1.4$.

Case I. $M = \frac{1}{11}$. The initial data for this test case are

$$\begin{aligned} \rho(x, 0) &= \bar{\rho}_0 + M\tilde{p}_0^{(1)} \tfrac{1}{2}(1.0 - \cos(2\pi x/L)) \\ p(x, 0) &= \bar{p}_0 + M\tilde{p}_0^{(1)} \tfrac{1}{2}(1.0 - \cos(2\pi x/L)) \\ u(x, 0) &= \mathrm{sign}(x)\tilde{u}_0 \tfrac{1}{2}(1.0 - \cos(2\pi x/L)) \end{aligned} \tag{4.1}$$

for $-L \leq x \leq L = 2/M$, where

$$\bar{\rho}_0 = 0.955, \bar{p}_0 = 1.0,$$

and

$$\tilde{\rho}_0^{(1)} = 2.0, \tilde{p}_0^{(1)} = 2\gamma, \tilde{u}_0 = 2\sqrt{\gamma}. \tag{4.1a}$$

We prescribe periodic boundary conditions which in the present case are equivalent to reflecting (rigid wall-) boundaries due to the symmetry in the initial data. The data from (4.1) approximate two acoustic pulses, one right-running pulse in $-L \leq x \leq 0$, and an antisymmetric left-running pulse in $0 \leq x \leq L$. The following numerical computations use 220 grid points within the interval from (4.1). Figures 4.1a, b show the pressure distributions at times $t = 0.815$ and $t = 1.63$. The initial data are also included for completeness. In Fig. 4.1a the pressure pulses have just collided and their super-position produces the maximum pressure of the computation. For comparison the figure shows the distributions obtained with the semi-implicit and with the second-order explicit scheme. The curves can hardly be distinguished. In Fig. 4.1b the pressure pulses have separated again. Weakly nonlinear acoustic effects have considerably distorted the profiles and weak shock formation is incipient. The solutions practically coincide in all of the domain, except for the vicinities of the locations $x \approx -18.5$ and $x \approx 18.5$, where shocks are beginning to form. In these regions the quality of the semi-implicit solution begins to deteriorate. This is not surprising, since we have built the scheme under the assumption of long wave acoustic solution components and this assumption is being violated in Fig. 4.1b. The deviations are due to the fact that we extract the first- and second-

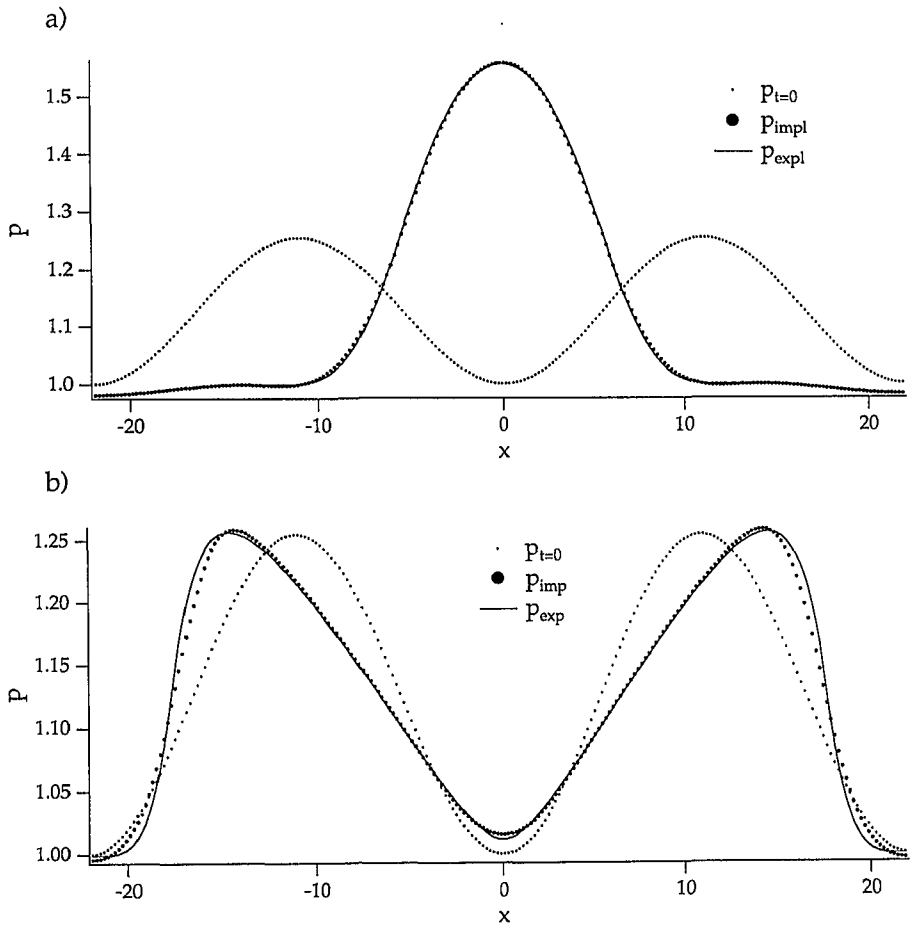

FIG. 4.1. Pressure profiles for the colliding acoustic wave problem from (4.1) with Mach number $M \simeq 0.1$: ..., initial distributions, ●, semi-implicit scheme (CFL $\simeq$ 5); ———, explicit MUSCL scheme (CFL = 0.8). (a) time, $t = 0.815$; (b) time, $t = 1.63$.

order pressures from the discrete pressure distribution by means of averaging procedures that involve $O(1/M)$ grid-points. In the vicinity of a developing discontinuity this produces an undesired smearing of the solution. We note that the scheme nevertheless does not produce spurious high-frequency oscillations. Several ways to improve the performance of the scheme on weak shock problems are currently being tested.

Figures 4.2a, b display the density distributions for Case I at the same times as mentioned before. The comparison with the solutions from the explicit scheme is as satisfactory as it was for the pressure. This is not trivial, since in the semi-implicit algorithm the density evolution is done by a completely different scheme than the pressure wave propagation. These results indicate that the interaction of these subschemes via Strang-type operator splitting produces the correct advection of the density when the flow is driven by acoustic waves.

A comparison of the computational efficiencies of the explicit and the semi-implicit calculations is given at the end of this section.

Case II. $M = \frac{1}{61}$. The initial data for this test case are

$$\begin{aligned} \rho(x,0) &= \bar{\rho}_0 + \Phi(x)\tilde{\rho}_0^{(0)} \sin(40\pi x/L) \\ &\quad + M\tilde{\rho}_0^{(1)}\tfrac{1}{2}(1.0 + \cos(\pi x/L)) \\ p(x,0) &= \bar{p}_0 + M\tilde{p}_0^{(1)}\tfrac{1}{2}(1.0 + \cos(\pi x/L)) \\ u(x,0) &= \tilde{u}_0\tfrac{1}{2}(1.0 + \cos(\pi x/L)) \end{aligned} \tag{4.2}$$

for $-L \le x \le L = 1/M$, with density coefficients

$$\bar{\rho}_0 = 1.0, \quad \tilde{\rho}_0 = 0.5, \tag{4.2a}$$

and the other parameters as in (4.1a). The function $\Phi(x)$ in $(4.2)_1$ is defined by

$$\Phi(x) = \begin{cases} 0, & -1/L \le x \le 0, \\ \frac{1}{2}(1.0 - \cos(5\pi x/L)), & 0 \le x \le 2L/5, \\ 0 & x > 2L/5, \end{cases} \tag{4.2b}$$

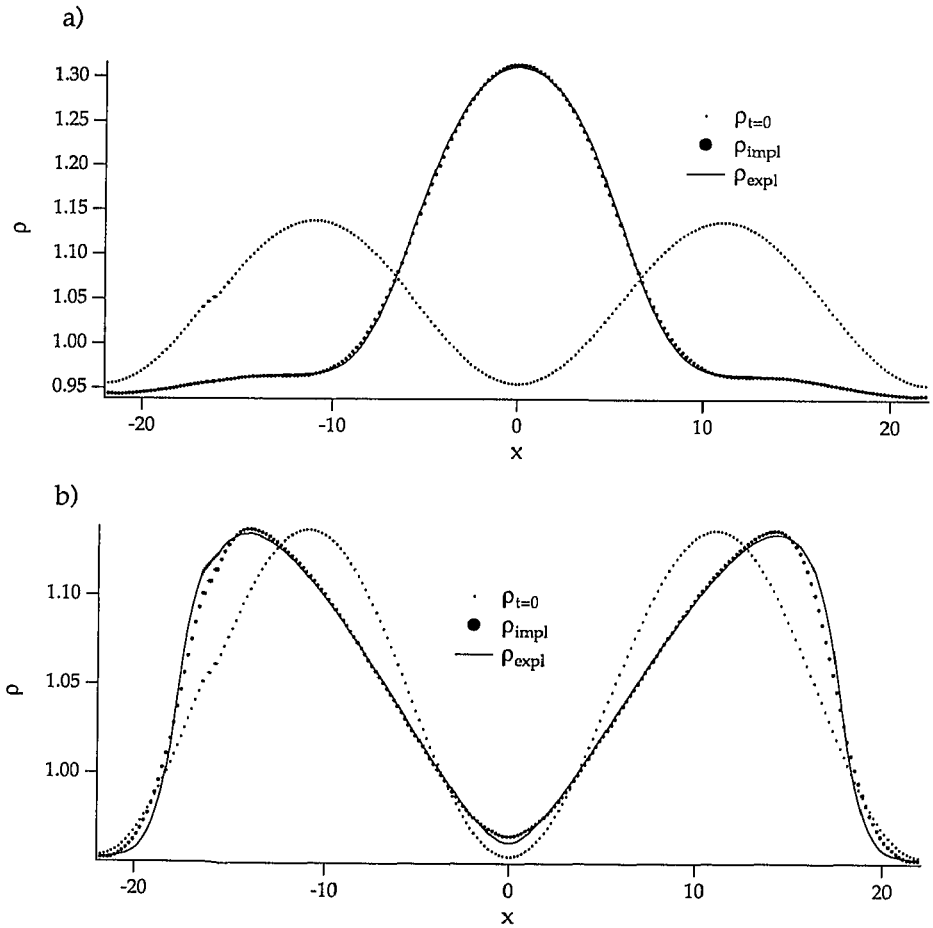

FIG. 4.2 Density profiles for the colliding acoustic wave problem from (4.1) with Mach number $M \simeq 0.1$: ...., initial distributions; ●, semi-implicit scheme (CFL $\simeq$ 5); ———, explicit MUSCL scheme (CFL = 0.8). (a) time, $t = 0.815$; (b) time, $t = 1.63$.

and smoothly restricts the large amplitude short wave length density fluctuations represented by $\tilde{\rho}_0$ to a region with length $2L/5$ to the right of the origin. This case operates with periodic boundary conditions.

The data from (4.2) represent a large amplitude, short wave length density layering that is set in motion by a periodic train of long wave right-running acoustic pulses. The numerical solution uses 1020 grid points within the interval from (4.2), which corresponds to about 25 gridpoints within a half-period of the small scale density layering.

Figures 4.3a, b and 4.4a, b show the pressure, velocity, and density distributions at time $t = 5.071$ after about two and a half turn-arounds of the long acoustic wave, together with the initial data. Again we have included the solutions from the explicit and from the semi-implicit schemes. First we observe from the pressure distribution in Fig. 4.3a that again the weakly nonlinear acoustic wave is described equally well by both schemes. The key aspect, however, of this example is the advection of the density profile due to the recurring interaction with the acoustic wave. The theoretical prediction is that the density fluctuation amplitude should be preserved in the process and that only small amplitude long wave variations should occur due to the adiabatic compression as the acoustic wave passes by. Besides this, the density layering should just move to the right, driven by the cumulative influence of the acoustic pulses. In Fig. 4.4a we observe that the semi-implicit scheme has quite accurately preserved the density fluctuation amplitudes over 189 time steps. We have used the Superbee limiter [28] to achieve these results. The explicit scheme, run with the same limiter, does not perform as well as is seen in Fig. 4.4b. This is due to the fact that the explicit scheme requires 4086 time steps to reach the same physical time and the small but nonzero dissipation of the scheme accumulates to reduce the total density variation by a factor of one-half.

Another aspect of this example is that at the location of the density fluctuations $O(M^2)$ pressure variations occur when the acoustic wave passes by. These are accompanied by first-order fluctuations of the velocity as displayed in Fig. 4.3b. The small amplitude pressure variations are more clearly visible in the close-up view of the pressure distribution in the interval $0 \leq x \leq 20$ in Fig. 4.5a. The explicit and semi-implicit computations show similar small amplitude variations, but due to the $O(1)$

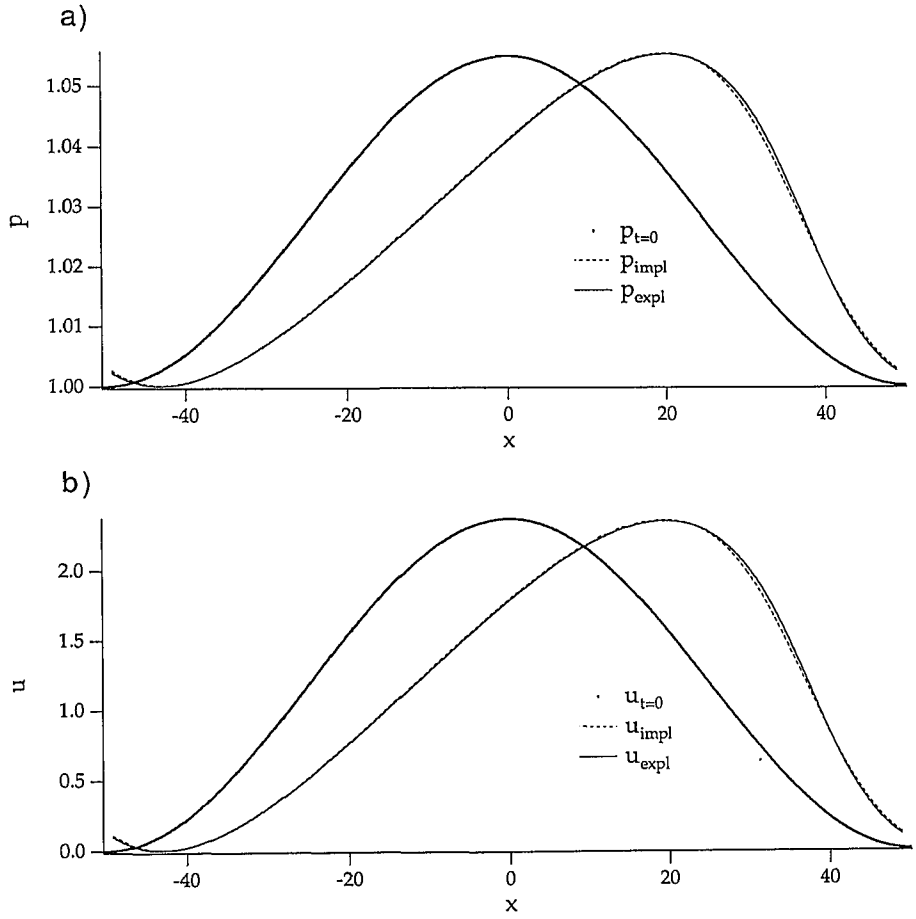

FIG. 4.3. Numerical solutions for the acoustic wave/density layer problem from (4.2) with Mach number $M \simeq 0.02$ at time $t = 5.071$: ..., initial distributions; ---, semi-implicit scheme (CFL $\simeq$ 22); ———, explicit MUSCL scheme (CFL = 0.8). (a) pressure distributions; (b) velocity distributions.

discrepancy between the densities, we cannot expect that the two pressure calculations coincide precisely. It is important to note that these $O(M^2)$ pressure variations must be obtained in the explicit calculation by delicate differences of $O(1)$ pressure data, while in the semi-implicit computation we compute separately the $O(M^2)$-pressure $\tilde{p}^{(2)}$, which resolves such small pressure variations consistently as $M \to 0$. Figure 4.5b displays $\tilde{p}^{(2)}$ at the same time $t = 5.071$, and we recognize its rapid variation at the location of the large density gradients.

A comparison of the computational efficiencies of the explicit and the semi-implicit calculations is given at the end of this section.

Case III. $M = 10^{-4}$. Here we consider the flow in an open tube, where mass with a given time dependent density is induced at the left end at a prescribed time dependent velocity. At the right end we prescribe a time dependent outflow pressure with large amplitude variation. Thus the initial and boundary conditions for this example read

$$(\rho, u, p)(x, 0) = (1.0, 1.0, 1.0), \tag{4.3a}$$

and

$$\begin{aligned} \rho(0, t) &= 1.0 + 0.3 * \sin(4.0 * t) \\ u(0, t) &= 1.0 + 0.5 * \sin(2.0 * t) \\ p(L, t) &= 1.0 + 0.25 * \sin(3.0 * t) \end{aligned} \tag{4.3b}$$

with $L = 10.0$. The Mach number for this example is $M = 10^{-4}$ and the effective Courant number for the numerical solution is CFL $\simeq 0.5 \times 10^4$. We resolve the computational domain by 100 grid points and, as a consequence, no long-wave acoustics with $O(l_{ref}/M)$ wave length can exist within the domain and the acoustic predictor for the implicit solution step is simply switched off. However, we do allow for a large amplitude background pressure variation as described in conjunction with (3.19b). Specifically, to provide a prediction for the total energy variation δe_i during the time step when entering the implicit step, we let

$$\delta e_i = \frac{\Delta t}{\gamma - 1} \left(\frac{dp_r}{dt} \right)^{(t^n + \delta t)}, \tag{4.4}$$

where $p_r(t) \equiv p(L, t)$. This term enters the second-order pressure

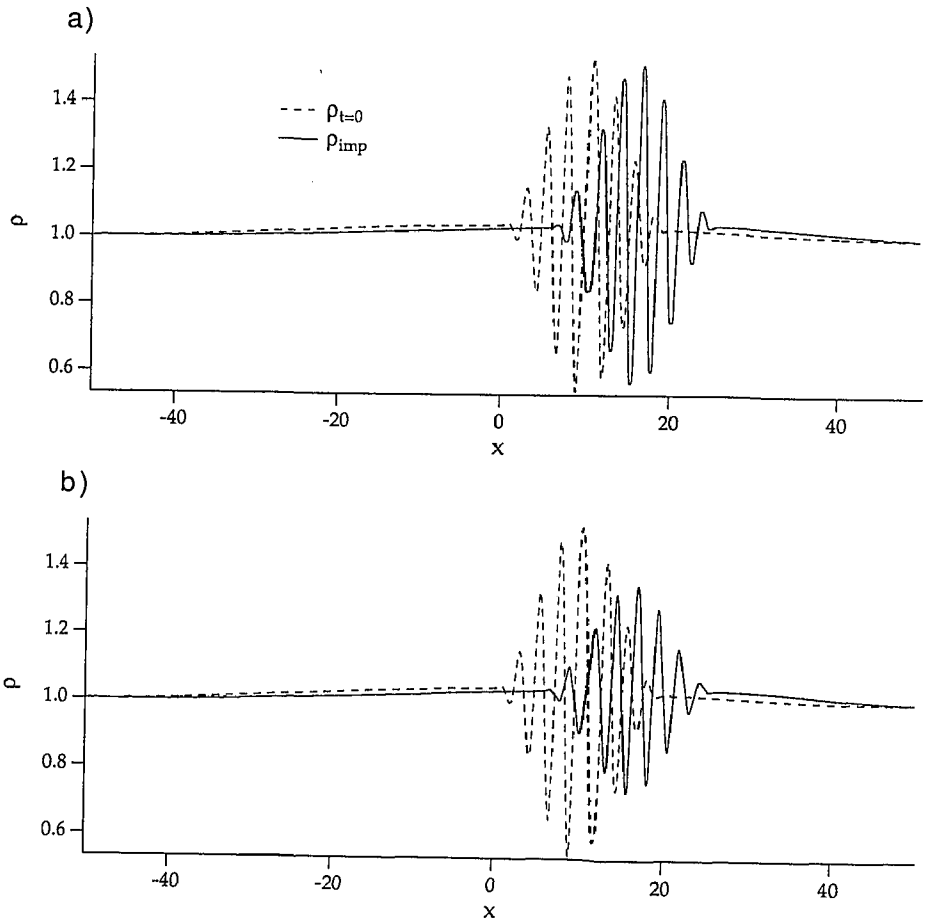

FIG. 4.4. Density profiles for the acoustic wave/density layer problem from (4.2) with Mach number $M \simeq 0.02$: ---, initial distributions; ———, numerical solution at time $t = 5.071$. (a) semi-implicit scheme (CFL $\simeq$ 22); (b) explicit MUSCL scheme (CFL = 0.8).

Poisson-type equation as a source term and it automatically generates the $\tilde{p}^{(2)}$-gradients needed to establish the flow divergence associated with the background compression. We describe the numerical treatment of the boundary conditions for this test problem in Appendix III.

Figures 4.6a, b and 4.7a, b show the second-order pressure, the flow velocity, and the density profiles at times $t = 6.56$ and 7.47 for this example. The limit solution as $M \to 0$ for this problem has been included for comparison. It can be computed by noting that u_x, due to (2.15) is a function of time only in one space dimension, which is prescribed when $p(L, t)$ from (4.3b) is inserted for P_0 (see the discussion below (2.16) in Section 2). Therefore the velocity is a linear function of x with given time dependent slope and boundary value at $x = 0$. According to (2.21) material elements undergo a quasi-static adiabatic compression and expansion while they follow the particle paths described by $u(x, t)$. With this, the leading order density and velocity and the leading and first-order pressure are known and we only need to determine the second-order pressure $p^{(2)}$. The latter follows from $(2.12)_3$ by a straightforward integration with respect to x in one space dimension. (The details are given in [31].)

We find very satisfactory agreement in all the profiles. In particular, the density distributions Figs. 4.6a, b show that mass-elements after entering the domain at the left end of the tube are correctly compressed and expanded in their further evolution. The global compression is clearly identified by the different density levels of the plateaus in the right half of the computational domain at the successive output times.

Computational Efficiencies. We summarize the effective computation times (for an HP 9000/735 workstation) and the numbers of time steps needed in the calculations for Cases I, II in Table I. We find that the key goal in developing a low-to-zero Mach number version of a compressible flow solver is achieved. The ratio of the numbers of time steps needed in an explicit computation versus that required in a semi-implicit run scales as $1/M$ for $M \to 0$. Due to the overhead of the semi-implicit scheme in comparison to the explicit version, the ratio of effective CPU times does not come out as favorably. The break-even point for the current

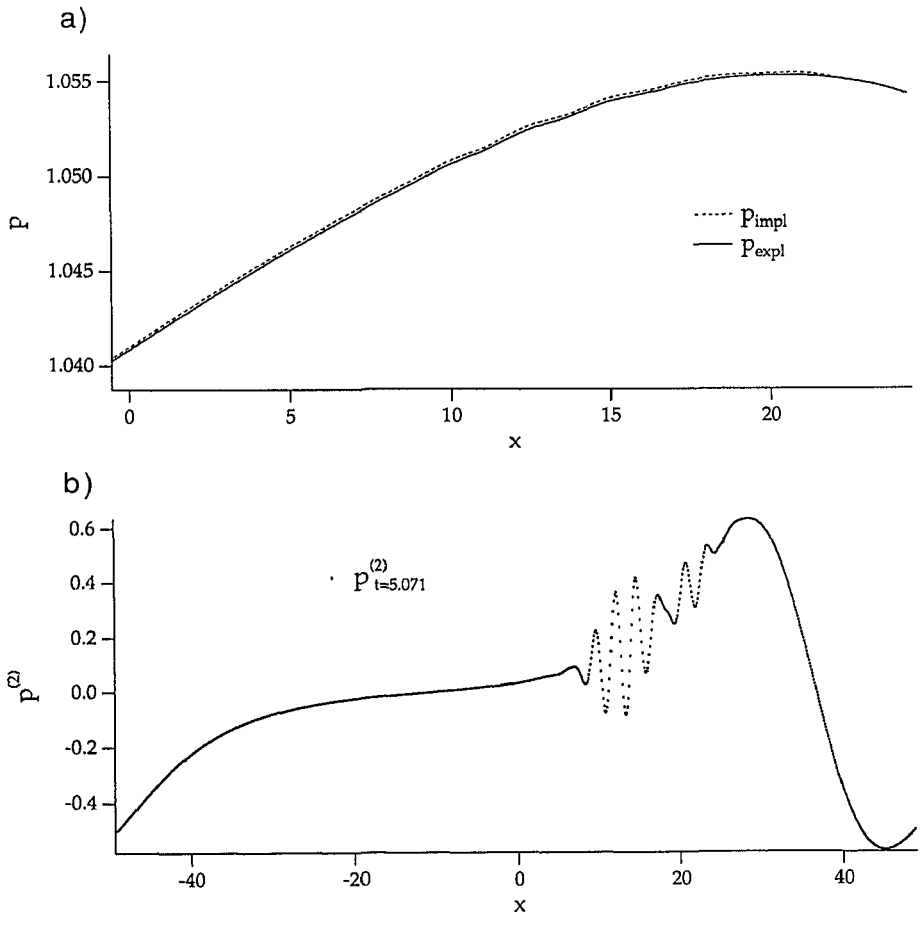

FIG. 4.5. Details of the pressure distributions for the acoustic wave/density layer problem from (4.2) with Mach number $M \simeq 0.02$ at time $t = 5.071$. (a) full pressure profiles in the vicinity of the density layering: ---, semi-implicit scheme (CFL $\simeq$ 22); ———, explicit MUSCL scheme (CFL = 0.8); (b) fluctuations of the second-order pressure, $\tilde{p}^{(2)}$, in the vicinity of the density layering from the semi-implicit computation.

version of the code and for one space dimension seems to occur at a Mach number of about $M = 0.1$. For Case II, where $M = 0.02$, the gain in computation time amounts to a factor of 4. This does not appear to be worth the effort in the first place, yet, we emphasize that:

(i) The semi-implicit computation, in addition to being faster, yields higher accuracy of the density profiles.

(ii) The current version of the semi-implicit scheme is not yet optimized for efficiency. The acoustic predictor based on LeVeque's large time step method is quite costly, due to the fact that during one time step each computational cell has to communicate with about $1/M$ neighbors. In fact, the estimates given in the table indicate that the acoustic predictor uses about 50% of the CPU time in the calculation for Case II. Promising, more efficient alternatives appear to be, [29],

— an implicit scheme based on the Crank–Nicholson discretization,

— a spectral method, or

— a *physically motivated multigrid approach* that describes the long wave solution components on a coarser grid.

(iii) Also, we reiterate that the solution scheme for System I (convection of mass and momentum) used here is a modified full compressible Euler solver, which takes about 34% of the CPU time in Case II. The goal here was to embed such a scheme in the overall code so that a reliable operation for large Mach numbers, i.e., fully compressible flows, would be guaranteed. If computational efficiency has the highest priority, one would switch to an algorithm optimized in that respect for sufficiently small Mach numbers.

(iv) The semi-implicit computations for Cases I, II were not performed with a time step near the stability limit of the scheme. In fact, a further extension of the time steps by a factor of 2 is possible, albeit with the cost of reduced accuracy. In that case, the computations take just about 12 and 85 time steps, respectively, and they are by a factor of two faster than indicated in the table. Yet, the accuracy of the solution is reduced.

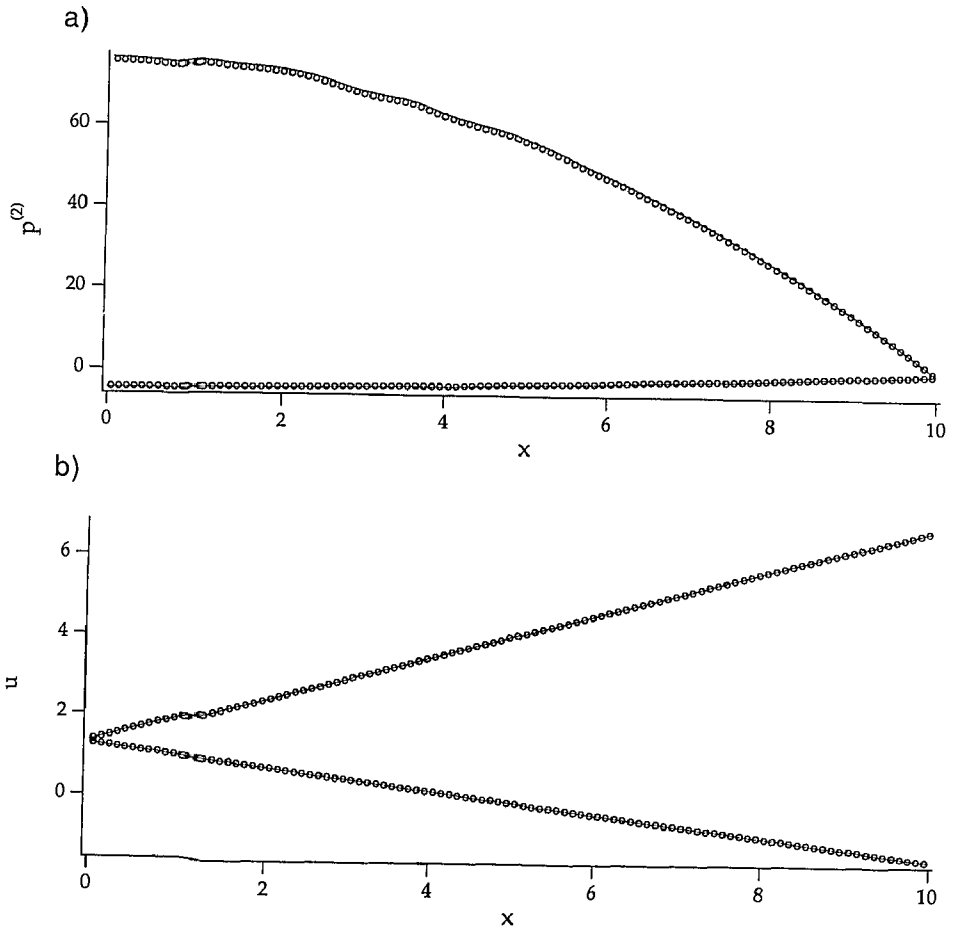

FIG. 4.6. Numerical solutions for the open tube problem with global compression from (4.3) with Mach Number $M \simeq 10^{-4}$ at times $t = 6.56, 7.47$: O, semi-implicit scheme (CFL $\simeq 0.5 \cdot 10^4$); ———, exact leading order asymptotic solution for M $\to$ 0. (a) pressure distributions; (b) velocity distributions.

5. REPORT ON EXISTING LITERATURE

5.1. *Multiple Scales—Low Mach Number Asymptotics*

There is a wide range of different distinguished regimes for low Mach number asymptotics and each regime is distinguished by different physical mechanisms. Here we briefly sketch the key scaling assumptions and the most prominent results of a number of earlier publications and we contrast them with the present asymptotic analysis from Section 2.

Ebin [32], by an approach using operator theory, and Klainerman and Majda [13], using classical energy estimates, prove that low Mach number flows are close to incompressible flows when suitable restrictions are imposed on the initial (and boundary) conditions (see also the further references in these papers). They show that weakly compressible flows of a barotropic fluid ($p = p(\rho)$) in fact converge to a limiting incompressible flow as the Mach number vanishes, if

1. the flow field is divergence-free initially, except for perturbations that vanish as $M \to 0$,

2. the pressure is uniform initially except for perturbations of $O(M^2)$, and

3. a single characteristic length scale governs the initial data.

Besides proving convergence, Klainerman and Majda show that higher order perturbations, under the restrictions in 1–3 above and for some finite time on the convective time scale, are governed by a hierarchy of nonconstant coefficient, nonhomogeneous linearized acoustic equations. These perturbations, in particular, include rapid oscillations associated with the passage of acoustic waves over the convective length scales. In addition, they successfully analyze viscous flows with the same methodology for vanishing Mach number.

When pressure fluctuations of $O(M)$ are present initially, i.e., when the second constraint above is relaxed, convergence to an incompressible flow as $M \to 0$ is not proven. However, a uniform stability estimate was given by Klainerman and Majda [13], showing that a classical differentiable solution of the compressible flow equation exists for some finite time interval.

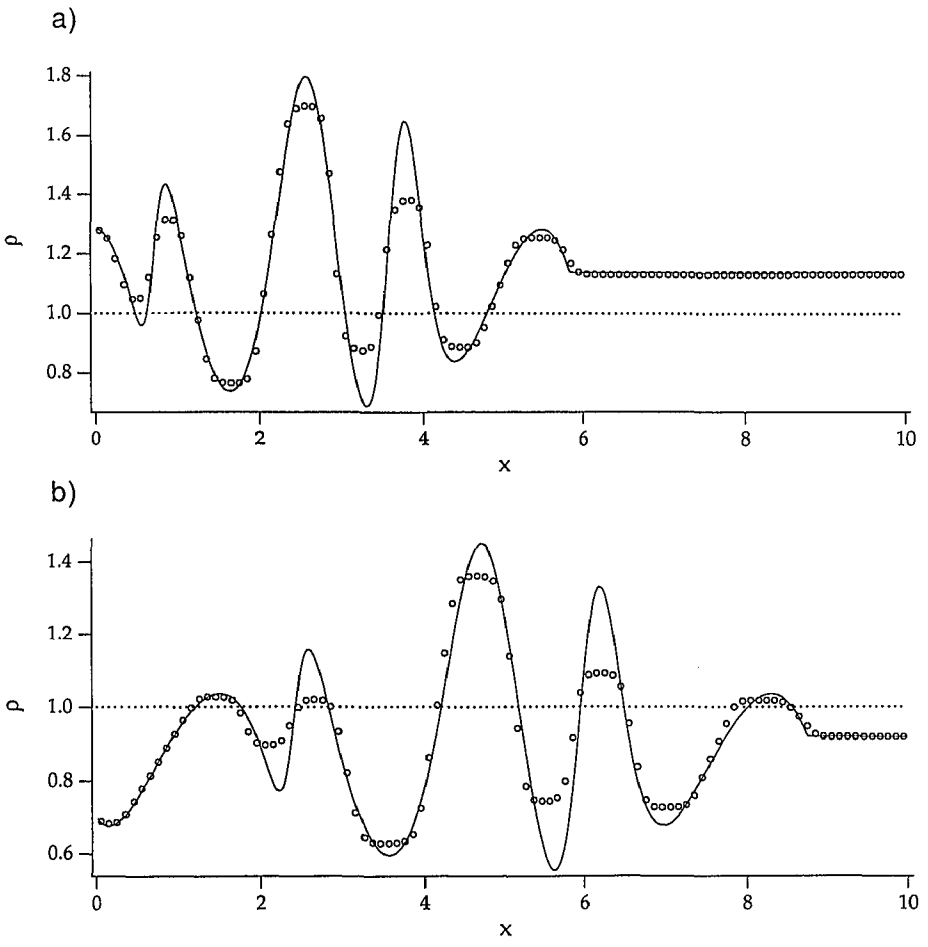

FIG. 4.7. Density distributions for the open tube problem with global compression from (4.3) with Mach number $M \simeq 10^{-4}$: O, semi-implicit scheme (CFL $\simeq 0.5 \cdot 10^4$); ———, exact leading order asymptotic solution for $M \to 0$. (a) time $t = 6.56$; (b) time $t = 7.47$

This classical solution is characterized by bounded velocities, pressure fluctuations no larger than $O(M)$, accelerations of order $O(1/M)$, and time changes of pressure of O(1). These bounds correlate with the intuitive expectations that single length scale initial data including O(M) pressure variations will (i) produce acoustic perturbations that affect the velocity at leading order (so that a proof of convergence to the incompressible limit is not available) and (ii) generate rapid acoustic oscillations of the velocity corresponding to the acceleration estimate $|\mathbf{v}_t| = O(1/M)$ as $M \to 0$.

The assumption of a barotropic fluid, where a direct relation $p = p(\rho)$ between pressure and density exists, restricts the analysis to constant-entropy data and the limiting case is constant density incompressible flow. As mentioned before, large amplitude density fluctuations are crucial for an accurate description of reacting flows. Schochet [33] extends several of the results of Klainerman and Majda in this respect and shows convergence of weakly compressible to incompressible variable density flows under similar restrictions on the initial data as stated in 1–3 above. (For a summary of existing theoretical results and further recent developments cf. [17].)

Majda and Sethian [14] and Majda and Lamb [18] perform a formal asymptotic analysis of *reactive* low Mach number flows. They derive a simplified set of equations for "zero Mach number combustion," which is the appropriate generalization of the equations of incompressible nonreacting flows. As in the

TABLE I

Comparison of Computational Efficiencies for Explicit and Semi-implicit Calculations on an HP 9000/735 Workstation, Including a Separate Count of the Percentage of CPU Time Used by the Several Split Operators in the Semi-implicit Computations

Case	Scheme	Time steps	CPU − secs.	% conv.	% acou.	% impl.
I	Expl.	128	0.58	100		
	Semi-impl.	25	0.52	48.4	24.8	26.8
II	Expl.	4084	83.15	100		
	Semi-impl.	188	22.86	34.0	49.5	16.5

studies before, pressure fluctuations are bounded to be $O(M^2)$ as $M \to 0$ with the consequence that acoustic effects are absent from the set of leading order equations. For rigorous results concerning well-posedness and short-time existence of these limit equations see Embid [34, 35].

A somewhat different approach has been chosen in a sequence of papers by Kreiss [36] and Tadmor [37]. Their fundamental notion is that in many applications one is not interested in high-frequency effects, but rather in the long time evolution of a system. For fluid mechanics this means to suppress rapid acoustic oscillations and to focus on the underlying quasi-incompressible flow. The goal in these studies is to derive constraints on the initial data that would guarantee the absence of high frequency solution components to some prechosen high perturbation order. The questions of whether these conditions can be met with some probability in reality and under which conditions the high frequency components—if present—would nontrivially affect the leading order solution structure remain open. The present assumption of long wave acoustic solution components for Cases I and II in Section 4 represents a way of "preparing the initial data" by imposing a particular multiple length scale structure that has not been considered previously.

All the analyses discussed so far assumed that the characteristic spatial scale of solutions is independent of the Mach number as $M \to 0$. The consequence is that under the assumption of a single evolution time scale for the leading order flow, acoustic effects can be allowed only as higher order corrections. For certain applications in combustion, in particular explosion processes that start with slow burning and then continuously accelerate to become fully compressible, this restriction is unacceptable. It is in fact the acoustics generated by the combustion heat release which is responsible for the flow acceleration. This was the motivation for the present analysis in Section 2. Here *long wave* acoustics with pressure wave amplitudes of $O(M)$ and leading order velocity contributions are allowed for. The long wave assumption guarantees that there is still only one governing characteristic time scale for all the processes involved.

A quite different regime is considered by Hunter *et al.* [15] (see also references therein), in which detailed effects of weakly nonlinear acoustics are prominent. A multiple time-multiple length scale analysis is performed that reveals weakly nonlinear acoustic wave deformation and resonant interactions of high frequency acoustics with entropy as well as vorticity perturbations. The basic underlying assumptions on the multiple scales structure of the solutions are as follows: On the shortest length scale—borrowing from the theory of geometrical optics—the solutions are composed of interacting *quasi-one-dimensional* wave fronts. A set of scalar phase functions $\theta_j(\mathbf{x}, t)$, varying only on the larger length scale, is introduced and the short wave length structure of the solution is associated with level sets of these phase functions:

$$\underline{u}(\mathbf{x}, t; M) = \underline{u}_0 + \sum_j \sigma_j \left(\frac{\theta_j(\mathbf{x}, t)}{\varepsilon}, \mathbf{x}, t \right) \underline{r}_j(\mathbf{x}, t). \quad (5.1)$$

The tangent vectors $\underline{r}_j(\mathbf{x}, t)$ in state space represent entropy, vorticity, and acoustic modes. Rapid variation occurs according to (5.1) only normal to level surfaces $\theta_j = \text{const.}$, while the variation of the wave amplitude σ_j in the tangential direction is slow. The result of this ansatz is a theory of multidimensional high frequency interactions of locally quasi-one-dimensional waves. (For further studies of this asymptotic regime, also in the context of combustion applications see [38, 39, 16, 40].) The scaling assumptions in this ansatz differ considerably from those considered in Section 2. Here we do allow for a quite general small scale solution structure that is not restricted to a superposition of quasi-one-dimensional modes, yet we only consider *long wave* acoustics with wave lengths *asymptotically large,* compared to the scales of the underlying quasi-incompressible flow.

We finally mention the very interesting work of Weinan E [19], whose length scaling is effectively the same as that considered here. The author considers *large amplitude* multiple length scale data for compressible flows in one space dimension. He shows that high frequency large amplitude acoustic modes will rapidly decay due to shock formation and the associated dissipation. One is then left with a multiple scales solution structure, where large amplitude density (entropy) fluctuations persist, while the inherently compressible acoustic contributions are either long wave or small amplitude. The author then derives new effective evolution equations for both the underlying small scale structure and the long wave–large amplitude gasdynamics. He obtains and rigorously justifies homogenized effective equations for the large scale flow that resembles the standard gasdynamics equations, yet with a homogenized entropy function that depends on the small scale solution structure. Since the author is interested in large amplitude effects, the question of the low Mach number limit behavior is not addressed, but since he does introduce the same spatial scaling assumptions as we have introduced in Section 2, a comparison and unification of both analyses seems very worthwhile.

5.2. *Review of Numerical Approaches to the Low Mach Number Problem*

Here we discuss approaches to solving the *full* compressible flow equations in the low Mach number regime. Thus, we do not address the wide range of publications proposing numerical schemes for the zero Mach number limit system, in which truly compressible effects are essentially suppressed, while density changes are still allowed. Nonetheless, this literature will be of utmost importance in our further work, as it contains a vast amount of analyses and experience in the design of higher order accurate schemes simulating flows with a divergence constraint (which is a highly nontrivial task!) [21, 41, 30].

The analysis in Section 2 has revealed three key issues that need to be addressed in designing a low Mach number flow computation scheme:

1. The dynamic range problem associated with the asymp-

totic pressure decomposition $p = p^{(0)} + Mp^{(1)} + M^2p^{(2)}$ and the fact that each of the $p^{(i)}$ affects the leading order velocity field.

2. The correct identification of singular and nonsingular terms in the flow equations as $M \to 0$. In particular, we argued that the "stiff" part of the equations should be hyperbolic with signal speeds $\lambda = c(1 + o(1))$ as $M \to 0$, if acoustic wave propagation is to be represented accurately.

3. The possibility of nonhomentropic flow, i.e., of variable densities. A particular consequence of large amplitude entropy fluctuations is that the speed of sound inherits these large amplitude variations. In addition, a numerical scheme for such applications must involve a mechanism for advection of entropy (or density).

We summarize in the following several earlier attempts at overcoming the numerical low Mach number problems and discuss these approaches in the light of items 1–3 above.

Casulli and Greenspan [3] perform a characteristic analysis of the Euler equations and identify those terms that are responsible for introducing the large speed-of-sound contribution to the signal speeds. They single out the pressure gradient in the momentum equation and the velocity divergence term in the energy equation in agreement with our asymptotic analysis. They then suggest building a semi-implicit discretization that treats only these terms implicitly, while handling the others explicitly. This approach allows them to face the issues 2 and 3 above (large signal speeds of the stiff part and variable densities), yet there is no pressure decomposition. Thus, their pressure variable must at the same time represent leading order thermodynamic effects and the small $O(M^2)$ pressure fluctuations responsible for the divergence constraint as $M \to 0$. As a consequence, their scheme does not automatically extend to zero Mach number. Patnaik *et al.* [4] extend a flux-corrected-transport (FCT) algorithm for compressible flows based on Casulli and Greenspan's ideas. Their results for acoustic wave propagation in a closed 1D-system exhibit strong damping when Courant numbers w.r.t. the sound speed larger than unity are used. This demonstrates the importance of our explicit linear acoustic predictor, in addition to the pressure decomposition, in obtaining very low dissipation for the long wave length acoustics.

Abarbanel *et al.* [6] argue, by providing some explicit examples, that a successful splitting of the compressible flow equations for small Mach numbers should involve split fluxes whose Jacobian matrices are simultaneously symmetrizable. Introducing a suitable variable transformation (entropy variables), they first symmetrize the Euler equations and then decompose the resulting symmetric coefficient matrices in stiff and nonstiff symmetric components. The stiff parts are linear, so that the associated split steps can be solved efficiently by an implicit method. The splitting is also shown to be stable when a time step restriction based on the flow velocity (not on the speed of sound) is introduced. Unfortunately, the approach draws heavily on the assumption that fluctuations of the speed of sound obey an estimate

$$\frac{c - c_\infty}{c_\infty} = o(1) \quad \text{as} \quad M \to 0, \tag{5.2}$$

where c_∞ is a constant reference speed of sound. This is true only for homentropic flows and, as a consequence, the method is not applicable to variable density flows. In addition, the stiff parts of the split operators have incorrect signal speeds in the limit, so that an accurate representation of acoustic wave propagation cannot be expected. The dynamic range problem for the pressure *is* overcome, albeit under the assumption of homentropic flow.

Gustafsson and co-workers [9] follow a similar route, but by using a different variable transformation for the symmetrization, they obtain split fluxes that do have the correct signal speeds as $M \to 0$. As regards the issues of variable density capacities and the dynamic range problem the same criticism as given above for Abarbanel *et al.* holds.

Sesterhenn *et al.* [10] introduce a heuristic splitting that separates the pressure gradient in the momentum equation from the rest of the terms. The surprising result is that the split systems in a characteristic analysis turn out to have the signal speeds $\{u, \gamma u, u\}$ for the step involving convection and $\{0, 0, -(\gamma - 1)u\}$ for the split step involving the pressure gradient. Obviously, the stiffness of the system is gone, as the speed of sound does not appear anymore. Hence, one is tempted to just use an explicit discretization for any Mach number. The authors show that, even though the separate steps are nonstiff, an explicit split step algorithm still suffers from a severe time step restriction. The splitting itself in this case introduces an instability that can be cured only by choosing sufficiently small time steps. This is in line with observations by Abarbanel *et al.* [6], who provide explicit examples demonstrating that this situation can easily occur for many hyperbolic systems. Sesterhenn *et al.* then discretize the pressure gradient contribution implicitly and downwind with respect to the flow velocity. This discretization is shown to be stabilizing. The approach yields promising results for steady flows, where the semi-implicit discretization allows large time steps and fast convergence. Yet, the signal speeds associated with the second step are incorrect and do not represent the acoustic signal speed. Hence, one may not expect accurate results for unsteady problems involving (long wave) acoustics.

SIMPLE-type algorithms (SIMPLE [2]; SIMPLEC; see Noll [42]) in principle are semi-implicit discretizations of the compressible flow equations which can be tuned to survive the zero Mach number limit. By dividing the time update into an explicit part and an implicit part, where the first step includes the effects of the pressure at the old time level, while the second accounts for the pressure update, one has a pressure decomposition quite similar to the present multiple pressure approach without explicitly saying so. One crucial ingredient is missing in these schemes, though, namely a separate scaling of these two pressure contributions: If the zero Mach number limit is to be achieved, then the explicit pressure terms must be scaled by a

suitable reference pressure p'_{ref}, while the pressure correction must be scaled with $\rho'_{\text{ref}}u'^2_{\text{ref}}$. Then, expressed in terms of our asymptotic analysis, the explicit pressure terms may be identified with the homogeneous background pressure $P_0(t)$, while the pressure corrections will correspond to $p^{(2)}(\mathbf{x}, t)$ as $M \to 0$.

The implicitly discretized terms of the SIMPLE-type schemes have the correct signal speeds as $M \to 0$, so that unsteady acoustic effects can be described, albeit with considerable dissipation as long as a suitable pressure scaling and special discretizations for acoustic effects are absent.

Another crucial difference between the SIMPLE-type and the present scheme is that the pressure correction equation in the former is obtained by replacing density changes in the *continuity equation* with pressure (and entropy) changes using the equation of state. For homentropic flows this approach is for all practical purposes identical with one that uses the energy equation to this end. For variable density flows, however, the changes of density due to the advection of entropy are by orders of magnitude larger than those due to the pressure variation. Extracting the correct information on pressure changes from the continuity equation then becomes an extremely subtle task. Also, an additional equation for, e.g., the temperature representing the entropy fluctuations must be solved. We hope to have pointed out sufficiently clearly in the preceding sections that in a finite volume approach the natural equation for describing the advection of entropy is the continuity equation, while the energy equation automatically yields the divergence constraint and should be used to obtain the Poisson-type equation for the "incompressible pressure" $p^{(2)}$.

The more recent SIMPLER version of the SIMPLE scheme [2] is computationally advantageous in comparison with the pressure correction schemes, yet a step in the "wrong" direction as regards a smooth approach to the zero Mach number limit. In this version, the implicit step uses not a pressure update, but the total pressure, thereby destroying the possibility of a suitable pressure rescaling for part of the scheme. As pointed out before, an algorithm that only knows one pressure variable will not be able to actually compute both compressible and truly incompressible flows due to the dynamic range problem (see item 1 at the beginning of this subsection).

Zienkiewicz *et al.* [8] propose an "all Mach number scheme" that is very similar to the SIMPLE-type algorithms with pressure correction but uses finite element type discretizations.

Colella [30] describes recent efforts aimed at numerically solving the equations of zero Mach number combustion (see [18]) by extending higher order projection methods [43, 44] for incompressible flows (see also [21, 41]). These schemes achieve higher order accuracy by employing Godunov-type upwind discretization ideas for describing convection of mass, momentum, and chemical species and sophisticated algorithms for the projection step. The use of Godunov-type discretizations, however, differs fundamentally from what is done in the present paper to solve the split System I from Section 3. We emphasize that in the references cited the asymptotic limit equations are solved rather than the full equations in a limit regime. Thus, e.g., acoustic effects are completely suppressed or computed by postprocessing as higher order corrections in the sense of Klainerman and Majda [13].

APPENDIX I: HLLE-FLUXES FOR THE EXPLICIT CONVECTION STEP

I.1. *Characteristic Analysis*

We write the auxiliary system I* from (3.8) as

$$\begin{aligned} \rho_t + m_x &= 0 \\ m_t + \left(\frac{m^2}{\rho} + p\right)_x &= 0 \\ e_t + (u[e + \pi])_x &= 0, \end{aligned} \tag{I.1}$$

where

$$\pi = \bar{\bar{p}}_{\text{NL}} + M^2 p, \tag{I.2}$$

and $\bar{\bar{p}}_{\text{NL}}$ is considered given and fixed in the characteristic analysis of (I.1) which shows that the system is strictly hyperbolic with eigenvalues

$$\lambda^0_* = u = \frac{m}{\rho}, \quad \lambda^{\pm}_* = u \pm c_*, \tag{I.3}$$

where

$$c^2_* = c^2 + \frac{\pi - p}{\rho^2 E_p}, \tag{I.4}$$

provided that

(i) $p_e\pi_\rho - \pi_e p_\rho = 0$

(ii) $p_e\pi_m - \pi_e p_m = 0$

(ii) $p_m + u\pi_e = 0.$

In (I.4) the quantity E is the internal energy per unit mass, i.e.,

$$E = \frac{1}{\rho}\left[e - M^2\frac{m^2}{2\rho}\right] = E(p, \rho) \tag{I.5}$$

and

$$c^2 = -\frac{E_\rho - p/\rho^2}{E_p} \tag{I.6}$$

is the unmodified (nondimensional) speed of sound of the gas. We note that conditions (i), (ii) are satisfied given the definition of π in (I.2) and with the assumption that $\bar{\bar{p}}_{\text{NL}}$ is considered

fixed. In addition we emphasize that this analysis holds as stated for general equations of state $E = E(p, \rho)$.

For the definition of the HLLE-fluxes we also need the left and right eigenvectors of system (I.1) associated with the λ^0_*-characteristic, i.e., with pure convection:

$$\underline{l}^0 = \frac{1}{c_*^2 E_p}\left(-\frac{e+\pi}{\rho} + M^2u^2, -M^2u, 1\right)$$
$$\underline{r}^0 = \begin{pmatrix} 1 \\ u \\ E + \rho E_\rho + \dfrac{M^2u^2}{2} \end{pmatrix}. \tag{I.7}$$

I.2. *Harten–Lax–van Leer–Einfeldt Fluxes*

System I*, i.e., (I.1), is equivalent to

$$\underline{u}_t + \underline{f}(\underline{u})_x = 0, \tag{I.8}$$

where $\underline{u} = (\rho, m, e), \underline{f}(\overline{u}) = (m, m^2/\rho + p, (m/\rho)[e + \pi])$. Here we describe how to construct numerical approximations, $\underline{g}(\underline{u}_l, \underline{u}_r)$, of the physical fluxes at the interfaces of the numerical grid cells, given two adjacent states, $\underline{u}_l, \underline{u}_r$. These are used in a standard fashion in a conservative discretization of the system of conservation laws in (I.8).

Let $\underline{f}_l = \underline{f}(\underline{u}_l), \underline{f}_r = \underline{f}(\underline{u}_r)$ be the exact fluxes associated with $\underline{u}_l, \underline{u}_r$, then the Harten–Lax–van Leer numerical flux is [25, 26]

$$\underline{g}^{\mathrm{HLL}}(\underline{u}_l, \underline{u}_r) = \frac{1}{b_r - b_l}\{b_r\underline{f}_l - b_l\underline{f}_r + b_lb_r(\overline{u}_r - \underline{u}_l)\}, \tag{I.9}$$

where b_l, b_r are approximations to the smallest and largest signal speeds associated with the Riemann Problem with initial data $\underline{u}_l, \underline{u}_r$.

For the original gasdynamic system, Einfeldt suggests the choices for b_l, b_r,

$$b_l = \min(\lambda_l^-, \lambda_{\mathrm{ROE}}^-, 0),$$
$$b_r = \max(\lambda_l^+, \lambda_{\mathrm{ROE}}^+, 0), \tag{I.10}$$

where $\lambda_{l,r}^{\pm}$ are the speeds for left and right running sound waves, $\lambda_{\mathrm{ROE}}^{\pm}$ are the corresponding Roe eigenvalues for $\underline{u}_l, \underline{u}_r$ (see, e.g., [28, 12]). The choice in (I.10) guarantees correct behavior with minimal dissipation for shock waves and, through the comparison with the smallest and largest characteristic speeds associated with $\underline{u}_l, \underline{u}_r$, respectively, it has a built-in entropy-fix that inhibits unphysical entropy-violating expansion shocks.

An important feature of the HLL-approach is that for an appropriate choice of the signal speeds one formally obtains a consistent upwind scheme. Small variations of b_l, b_r do not affect the performance of the scheme and its numerical dissipation. We have used this fact by defining the relevant signal speeds for the numerical fluxes of system I* as

$$b_l^* = \min((u - c)_l, (u - c)_{\mathrm{ROE}}, 0),$$
$$b_r^* = \max((u + c)_l, (u + c)_{\mathrm{ROE}}, 0), \tag{I.11}$$

where u_{ROE}, c_{ROE} are obtained in the usual fashion as

$$u_{\mathrm{ROE}} = \frac{u_r\sqrt{\rho_r} + u_l\sqrt{\rho_l}}{\sqrt{\rho_r} + \sqrt{\rho_e}}, \tag{I.12}$$

$$c_{\mathrm{ROE}} = \sqrt{(\gamma - 1)(H_{\mathrm{ROE}} - M^2u_{\mathrm{ROE}}^2/2)}, \tag{I.13}$$

$$H_{\mathrm{ROE}} = \frac{H_r\sqrt{\rho_r} + H_l\sqrt{\rho_l}}{\sqrt{\rho_r} + \sqrt{\rho_e}}, \tag{I.14}$$

$$H = \frac{e+p}{\rho}. \tag{I.15}$$

Einfeldt [26] observes that the HLL scheme as described operates quite dissipatively on contact discontinuities. He suggests an improvement that modifies the fluxes in (I.9) by an additional component proportional to the right eigenvector(s) associated with the u-characteristic.

$$\underline{g}^{\mathrm{HLLE}} = \underline{g}^{\mathrm{HLL}} + \eta(\underline{l}^0 \cdot (\underline{u}_r - \underline{u}_l))\underline{r}^0, \tag{I.16}$$

where

$$\eta = \frac{b_r - b_l}{2b_r}. \tag{I.17}$$

Einfeldt shows that the modified scheme in (I.16) is equivalent to Roe's linearized solver except for a different entropy-fix.

This concludes the discussion of the numerical fluxes for System I*. We have implemented a second-order version of the scheme by using a standard MUSCL-type approach as described, e.g., in [45, 11, 12, 46].

APPENDIX II: LEVEQUE'S LARGE TIME STEP METHOD FOR THE LINEAR ACOUSTIC SYSTEM (3.16)

Given $(\overline{m}, \overline{p}^{(1)}, \overline{\overline{c}}^2)_j^n$, we compute for each cell interface, $j + \frac{1}{2}$, the amplitudes of left and right running acoustic pulse amplitudes, according to

$$\delta\sigma_{j+1/2}^{\pm} = \frac{1}{2}\left((\overline{m}_{j+1} - \overline{m}_j) \pm \frac{1}{\overline{\overline{c}}_{j+1/2}^2}(\overline{p}_{j+1}^{(1)} - \overline{p}_j^{(1)})\right), \tag{II.1}$$

where

$$\overline{\overline{c}}_{j+1/2}^2 = \tfrac{1}{2}(\overline{\overline{c}}_{j+1}^2 + \overline{\overline{c}}_j^2). \tag{II.2}$$

Then we distribute the acoustic perturbations over neighboring cells by

$$\delta\bar{m}_j = \sum_{i=j-1/M-1/2}^{j-1/2} w_{ij}^{+}\,\delta\sigma_i^{+}\underline{r}_i^{+} + \sum_{i=j+1/2}^{j+1/M+1/2} w_{ij}^{-}\,\delta\sigma_i^{-}\underline{r}_i^{-}. \quad \text{(II.3)}$$

Here the

$$\underline{r}_i^{\pm} = \begin{pmatrix} 1 \\ \pm\bar{\bar{c}}^2 \end{pmatrix} \quad \text{(II.4)}$$

are the right eigenvector of the linearized acoustic system (3.16) representing right and left running acoustic waves and the weights $w_{ij}^{\pm}$ are computed as follows: For a right-running acoustic pulse from the cell interface with index $i = j_i + \frac{1}{2}$, compute its location x_i^{+} after the time step as

$$x_i^{+} = x_i + \frac{1}{M}\bar{\bar{c}}_i\,\Delta t. \quad \text{(II.5)}$$

Then

$$w_{ij}^{+} = \begin{cases} 0, & x_i^{+} < x_{j-1/2} \\ \dfrac{1}{\Delta x}(x_i^{+} - x_{j-1/2}), & x_{j-1/2} \le x_i^{+} < x_{j+1/2} \\ 1, & x_{j+1/2} \le x_i^{+}. \end{cases} \quad \text{(II.6)}$$

Analogously,

$$x_i^{-} = x_i - \frac{1}{M}\bar{\bar{c}}_i\,\Delta t \quad \text{(II.7)}$$

and

$$w_{ij}^{-} = \begin{cases} 0, & x_i^{-} > x_{j+1/2} \\ \dfrac{1}{\Delta x}(x_{j+1/2} - x_i^{-}), & x_{j+1/2} \ge x_i^{-} > x_{j-1/2} \\ 1, & x_{j-1/2} \ge x_i^{-}. \end{cases} \quad \text{(II.8)}$$

This completes the description of the first-order algorithm that was employed for all the numerical examples of Section 4. For a higher order extension of the scheme and applications to general nonlinear systems, see [24].

APPENDIX III. BOUNDARY CONDITIONS FOR THE THIRD TEST PROBLEM FROM (4.3)

For the explicit convection step we employ the following standard approach: We introduce at both ends of the domain two dummy cells and, before applying the discrete solution operator, assign appropriate states to these cells, such that the explicit scheme automatically yields fluxes at the boundaries that are compatible with the desired boundary conditions.

Left boundary. Density and velocity are prescribed at the left boundary, so that their exact values, $(\rho_l, u_l)(t) \equiv (\rho, u)(x = 0, t)$, are known. Consider the nth convective computational step to be completed and let the subscripts $-1,0$ indicate the two dummy cells to the left of the computational domain, while the subscripts 1, 2, indicate the first two cells. Then we extrapolate the density and velocity profiles as

$$\begin{aligned} (\rho, u)_0^0 &= 2(\rho, u)_l(t^n) - (\rho, u)_1^0, \\ (\rho, u)_{-1}^0 &= 2(\rho, u)_l(t^n) - (\rho, u)_2^0, \end{aligned} \quad \text{(III.1)}$$

where the superscript ^{0} is defined in analogy with our notation of Section 3. The pressure is extrapolated using the values in cells 1, 2, by

$$\begin{aligned} (\partial p/\partial x)_0^0 &= (p_2^0 - p_1^0)/\Delta x \\ p_0^0 &= p_1^0 - \Delta x(\partial p/\partial x)_0^0, \quad p_{-1}^0 = p_2^0 - 3\,\Delta x\,(\partial p/\partial x)_0^0. \end{aligned} \quad \text{(III.2)}$$

For the implicit step we introduce a gradient boundary condition for the second-order pressure $\tilde{p}^{(2)}$. The idea is that the explicit step will typically not guarantee exact compliance of the numerical solution with the prescribed boundary condition and we need to enforce an additional acceleration at $x = 0$ to make up for the difference. Thus we let

$$\tilde{u}_l = \frac{1}{2}\left[\frac{(\rho u)_1}{\rho_1} + \frac{(\rho u)_0}{\rho_0}\right], \quad \text{(III.3)}$$

where the data used on the right-hand side are those obtained from the preceding explicit convection step. The gradient of the perturbation pressure at the left boundary is set to

$$\frac{\partial}{\partial x}(\tilde{p}^{(2)} - p)\big|_{x=0} = -\frac{\rho_l(t^{n+1})}{\Delta t}(u_l(t^{n+1}) - \tilde{u}_l). \quad \text{(III.4)}$$

Then approximations $\tilde{p}^{(2)}$ at x_0, x_{-1} are computed in analogy with the formulas in (III.2)$_2$.

At the right boundary all quantities, except for the second-order pressure, are linearly extrapolated. For the second-order pressure we use a quadratic extrapolation formula based on the gridpoint values at x_{im-1}, x_{im} and the additional constraint that $\tilde{p}^{(2)}(L, t) \equiv 0$. This provides the necessary right boundary condition for $\tilde{p}^{(2)}$ at x_{im+1} which is the first dummy point outside of the computational domain.

ACKNOWLEDGMENTS

The author is indebted to Dr. Claus Dieter Munz, Forschungszentrum Karlsruhe, Germany, for numerous valuable discussions and for his unceasing encour-

agement. Dr. Munz, in particular, provided crucial contributions in the formation stage of this research project, where the necessity for the introduction of multiple pressure variables and large scale averaging procedures in the semi-implicit scheme was discovered. Dipl.-Phys. Klaus Lange, Dipl.-Ing. Werner Willems, and Dipl.-Ing. Karl-Joseph Geratz, Institut für Technische Mechanik, RWTH Aachen, implemented a simplified version of the present low Mach number scheme (without acoustic predictor) in an existing three-dimensional flow solver and provided the results for the third test case in Section 4. In their work, a modified Harten/Lax/van Leer/Einfeldt scheme was employed for the first time in the explicit convection step. Their continuous feedback greatly accelerated the formulation of the implicit second-order pressure correction.

REFERENCES

1. J. H. S. Lee and I. O. Moen, *Prog. Energy Combust. Sci.* **6,** 359 (1980).
2. S. V. Patankar, *Numerical Heat Transfer and Fluid Flow* (Hemisphere, Washington, DC, 1980).
3. V. Casulli and D. Greenspan, *Int. J. Numer. Methods. Fluids* **4,** 1001 (1984).
4. G. Patnaik, R. H. Guirguis, J. P. Boris, E. S. Oran, *J. Comput. Phys.* **71,** (1987).
5. C. L. Merkle and Y.-H. Choi, *AIAA J.* **25,** 831 (1987).
6. S. Abarbanel, P. Duth, and D. Gottlieb, *Comput. & Fluids* **17,** 1 (1989).
7. G. Fernandez, Dissertation, l'université de Nice, 5 juin 1989.
8. O. C. Zienkiewicz, J. Szmeltzer, and J. Peraire, *Comput. Methods Appl. Mech. Eng.* **78,** 105 (1990).
9. B. Gustafsson and H. Stoor, *SIAM J. Numer. Anal.* **28,** 1523 (1991).
10. J. Sesterhenn, B. Müller, and H. Thomann, "Computation of Compressible Low Mach Number Flow," in Computational Fluid Dynamics, Vol. 2, edited by Hirsch *et al.* (Elsevier, 1992), p. 829.
11. B. van Leer, *J. Comput. Phys.* **14,** 361 (1979).
12. R. J. LeVeque, *Numerical Methods for Conservation Laws* (Birkhäuser, Basel, 1990).
13. S. Klainerman and A. J. Majda, *Commun. Pure Appl. Math.* **35,** 629 (1982).
14. A. J. Majda and J. Sethian, *Combust. Sci. Technol.* **42,** 185 (1985).
15. J. K. Hunter, A. J. Majda, and R. R. Rosales, *Stud. Appl. Math.* **75,** 187 (1986).
16. R. Klein and N. Peters, *J. Fluid Mech.* **187,** 197 (1988).
17. S. Schochet, preprint, School of Mathematics, Tel Aviv University, 1993.
18. A. J. Majda and K. Lamb, IMA Preprint Series No. 664, Inst. of Mathematics and its Applications, University of Minnesota, Minneapolis, 1990.
19. W. E., *Commun. Part. Differential Eqs.* **17,** 347 (1992).
20. M. Matalon and B. J. Matkowski, *J. Fluid Mech.* **124,** 239 (1982).
21. A. J. Chorin, *Math. Comput.* **22,** 745 (1968).
22. R. Klein and C. D. Munz, "The Multiple Pressure Variable (MPV) Approach for the Numerical Approximation of Weakly Compressible Fluid Flow," in *Proceedings, Intl. Conf. on Numer. Methods in Cont. Mech., Prague, June 1994,* to appear.
23. W. Schneider, *Mathematische Methoden in der Strömungsmechanik* (Vieweg, Wiesbaden, 1978).
24. R. J. LeVeque, *SIAM J. Numer. Anal.* **22,** 1051 (1985).
25. A. Harten, P. Lax, and B. van Leer, *SIAM Rev.* **25,** 35 (1983).
26. B. Einfeldt, *SIAM J. Numer. Anal.* **25,** 294 (1988).
27. J. F. Gerbeau, N. Glinsky-Olivier, and B. Larrouturou, in preparation, 1993.
28. P. L. Roe, *J. Comput. Phys.* **43,** 357 (1981).
29. R. Klein, and C. D. Munz, "The extension of incompressible flow solvers to the weakly compressible regime," to be submitted.
30. P. Colella, "High-Resolution Numerical Methods for Low Mach Number Flows," in *Proceedings, 5th Intl. Conf. on Hyperbolic Systems, SUNY, Stony Brook, June 1994,* to appear.
31. K. Lange, Diplomarbeit (Physik), Institut für Technische Mechanik, RWTH Aachen, 1993 (unpublished).
32. D. G. Ebin, *Commun. Pure Appl. Math.* **15,** 451 (1982).
33. S. Schochet, *J. Diff. Equations* **75,** 1 (1988).
34. P. Embid, *Commun. Partial Diff. Equations* **12,** 1227 (1987).
35. P. Embid, *Commun. Partial Diff. Equations* **19,** 1249 (1989).
36. H.-O. Kreiss, *Commun. Pure Appl. Math.* **33,** 399 (1980).
37. E. Tadmor, *Commun. Pure Appl. Math.* **35,** 839 (1982).
38. A. J. Majda, R. R. Rosales, and M. Schönbeck, *Stud. Appl. Math.* **79,** 205 1988.
39. A. J. Majda and R. R. Rosales, *SIAM J. Appl. Math.* **47,** 1017 (1987).
40. R. F. Almgren, *SIAM J. Appl. Math.* **51,** 351 (1991.
41. J. van Kan, *SIAM J. Sci. Stat. Comput.* **7,** 870 (1986).
42. B. Noll, *Numerische Strömungsmechanik* (Springer-Verlag, Berlin Heidelberg, 1993).
43. J. B. Bell, P. Colella, and H. M. Glaz, *J. Comput. Phys.* **85,** 257 (1989).
44. A. S. Almgren, J. B. Bell, P. Colella, and T. Marthaler, Lawrence Livermore Nat. Lab. Preprint UCRL-JC-118091, 1994.
45. C. D. Munz, "On the Comparison and Construction of Two-Step Schemes for the Euler Equations," in *Notes on Numerical Fluid Mechanics,* Vol. **14** (Vieweg, Wiesbaden, 1986).
46. P. Colella, *SIAM J. Sci. Stat. Comput.* **6,** 104 (1985).